

1 **Aqueous-phase mechanism for secondary organic aerosol formation from isoprene:**
2 **application to the Southeast United States and co-benefit of SO₂ emission controls**

3
4 E. A. Marais¹, D. J. Jacob^{1,2}, J. L. Jimenez^{3,4}, P. Campuzano-Jost^{3,4}, D. A. Day^{3,4}, W. Hu^{3,4}, J.
5 Krechmer^{3,4}, L. Zhu¹, P. S. Kim², C. C. Miller², J. A. Fisher⁵, K. Travis¹, K. Yu¹, T. F. Hanisco⁶,
6 G. M. Wolfe^{6,7}, H. L. Arkinson⁸, H. O. T. Pye⁹, K. D. Froyd^{3,10}, J. Liao^{3,10}, V. F. McNeill¹¹

7
8 ¹School of Engineering and Applied Sciences, Harvard University, Cambridge, MA, USA.

9 ²Earth and Planetary Sciences, Harvard University, Cambridge, MA, USA.

10 ³Cooperative Institute for Research in Environmental Sciences, University of Colorado, Boulder, CO, USA.

11 ⁴Department of Chemistry and Biochemistry, University of Colorado, Boulder, CO, USA.

12 ⁵School of Chemistry and School of Earth and Environmental Sciences, University of Wollongong, Wollongong,
13 New South Wales, Australia.

14 ⁶Atmospheric Chemistry and Dynamics Lab, NASA Goddard Space Flight Center, Greenbelt, MD, USA.

15 ⁷Joint Center for Earth Systems Technology, University of Maryland Baltimore County, Baltimore, MD, USA.

16 ⁸Department of Atmospheric and Oceanic Science, University of Maryland, College Park, MD, USA.

17 ⁹National Exposure Research Laboratory, US EPA, Research Triangle Park, NC, USA.

18 ¹⁰Chemical Sciences Division, Earth System Research Laboratory, NOAA, Boulder, Colorado, USA

19 ¹¹Department of Chemical Engineering, Columbia University, New York, New York 10027, USA.

20
21 **Abstract**

22 Isoprene emitted by vegetation is an important precursor of secondary organic aerosol
23 (SOA), but the mechanism and yields are uncertain. Aerosol is prevailingly aqueous under the
24 humid conditions typical of isoprene-emitting regions. Here we develop an aqueous-phase
25 mechanism for isoprene SOA formation coupled to a detailed gas-phase isoprene oxidation
26 scheme. The mechanism is based on aerosol reactive uptake coefficients (γ) for water-soluble
27 isoprene oxidation products, including sensitivity to aerosol acidity and nucleophile
28 concentrations. We apply this mechanism to simulation of aircraft (SEAC⁴RS) and ground-based
29 (SOAS) observations over the Southeast US in summer 2013 using the GEOS-Chem chemical
30 transport model. Emissions of nitrogen oxides ($\text{NO}_x \equiv \text{NO} + \text{NO}_2$) over the Southeast US are
31 such that the peroxy radicals produced from isoprene oxidation (ISOPO_2) react significantly with
32 both NO (high- NO_x pathway) and HO_2 (low- NO_x pathway), leading to different suites of
33 isoprene SOA precursors. We find a mean SOA mass yield of 3.3 % from isoprene oxidation,
34 consistent with the observed relationship of total fine organic aerosol (OA) and formaldehyde (a
35 product of isoprene oxidation). Isoprene SOA production is mainly contributed by two
36 immediate gas-phase precursors, isoprene epoxydiols (IEPOX, 58% of isoprene SOA) from the
37 low- NO_x pathway and glyoxal (28%) from both low- and high- NO_x pathways. This speciation is
38 consistent with observations of IEPOX SOA from SOAS and SEAC⁴RS. Observations show a
39 strong relationship between IEPOX SOA and sulfate aerosol that we explain as due to the effect
40 of sulfate on aerosol acidity and volume. Isoprene SOA concentrations increase as NO_x
41 emissions decrease (favoring the low- NO_x pathway for isoprene oxidation), but decrease more

42 strongly as SO₂ emissions decrease (due to the effect of sulfate on aerosol acidity and volume).
43 The US EPA projects 2013-2025 decreases in anthropogenic emissions of 34% for NO_x (leading
44 to 7% increase in isoprene SOA) and 48% for SO₂ (35% decrease in isoprene SOA). Reducing
45 SO₂ emissions decreases sulfate and isoprene SOA by a similar magnitude, representing a factor
46 of 2 co-benefit for PM_{2.5} from SO₂ emission controls. There is some evidence for this co-benefit
47 in observed long-term trends of OA in the Southeast US over the past decade.

48

49 Keywords: isoprene, SOA yield, IEPOX, glyoxal, SEAC⁴RS, SOAS, formaldehyde.

50

51 Corresponding Author: emarais@seas.harvard.edu

52 **1. Introduction**

53 Isoprene emitted by vegetation is a major source of secondary organic aerosol (SOA)
54 (Carlton et al., 2009, and references therein) with effects on human health, visibility, and climate.
55 There is large uncertainty in the yield and composition of isoprene SOA (Scott et al., 2014;
56 McNeill et al., 2014), involving a cascade of species produced in the gas-phase oxidation of
57 isoprene and their interaction with pre-existing aerosol (Hallquist et al., 2009). We develop here
58 a new aqueous-phase mechanism for isoprene SOA formation coupled to gas-phase chemistry,
59 implement it in the GEOS-Chem chemical transport model (CTM) to simulate observations in
60 the Southeast US, and from there derive new constraints on isoprene SOA yields and the
61 contributing pathways.

62 Organic aerosol is ubiquitous in the atmosphere, often dominating fine aerosol mass
63 (Zhang et al., 2007), including in the Southeast US where it accounts for more than 60% in
64 summer (Attwood et al., 2014). It may be directly emitted by combustion as primary organic
65 aerosol (POA), or produced within the atmosphere as SOA by oxidation of volatile organic
66 compounds (VOCs). Isoprene (C_5H_8) from vegetation is the dominant VOC emitted globally,
67 and the Southeast US in summer is one of the largest isoprene-emitting regions in the world
68 (Guenther et al., 2006). SOA yields from isoprene are low compared with larger VOCs (Pye et
69 al., 2010), but isoprene emissions are much higher. Kim et al. (2015) estimated that isoprene
70 accounts for 40% of total organic aerosol in the Southeast US in summer.

71 Formation of OA from oxidation of isoprene depends on local concentrations of nitrogen
72 oxide radicals ($NO_x \equiv NO + NO_2$) and pre-existing aerosol. NO_x concentrations determine the
73 fate of organic peroxy radicals originating from isoprene oxidation ($ISOPO_2$), leading to
74 different cascades of oxidation products in the low- NO_x and high- NO_x pathways (Paulot et al.,

75 2009a; 2009b). Uptake of isoprene oxidation products to the aerosol phase depends on their
76 vapor pressure (Donahue et al., 2006), solubility in aqueous media (Saxena and Hildeman,
77 1996), and subsequent condensed-phase reactions (Volkamer et al., 2007). Aqueous aerosol
78 provides a medium for reactive uptake (Eddingsaas et al., 2010; Surratt et al., 2010) with
79 dependences on acidity (Surratt et al., 2007a), concentration of nucleophiles such as sulfate
80 (Surratt et al., 2007b), aerosol water (Carlton and Turpin, 2013), and organic coatings (Gaston et
81 al., 2014).

82 We compile in Fig. 1 the published laboratory yields of isoprene SOA as a function of
83 initial NO concentration and relative humidity (RH). Here and elsewhere, the isoprene SOA
84 yield is defined as the mass of SOA produced per unit mass of isoprene oxidized. Isoprene SOA
85 yields span a wide range, from <0.1% to >10%, with no systematic difference between low-NO_x
86 and high-NO_x pathways. Yields tend to be higher in dry chambers (RH < 10%). Under such dry
87 conditions isoprene SOA is expected to be solid (Virtanen et al., 2010; Song et al., 2015). At
88 humid conditions more representative of the summertime boundary layer, aerosols are likely
89 aqueous (Bateman et al., 2014). Standard isoprene SOA mechanisms used in atmospheric models
90 assume reversible partitioning onto pre-existing organic aerosol, fitting the dry chamber data
91 (Odum et al., 1996). However, this may not be appropriate for actual atmospheric conditions
92 where aqueous-phase chemistry with irreversible reactive uptake of water-soluble gases is likely
93 the dominant mechanism (Ervens et al., 2011; Carlton and Turpin, 2013). Several regional/global
94 models have implemented mechanisms for aqueous-phase formation of isoprene SOA (Fu et al.,
95 2008, 2009; Carlton et al., 2008; Myriokefalitakis et al., 2011; Liu et al., 2012; Pye et al., 2013;
96 Lin et al., 2014).

97 Here we present a mechanism for irreversible aqueous-phase isoprene SOA formation
98 integrated within a detailed chemical mechanism for isoprene gas-phase oxidation, thus linking
99 isoprene SOA formation to gas-phase chemistry and avoiding more generic volatility-based
100 parameterizations that assume dry organic aerosol (Odum et al., 1996; Donahue et al., 2006). We
101 use this mechanism in the GEOS-Chem CTM to simulate observations from the SOAS (surface)
102 and SEAC⁴RS (aircraft) field campaigns over the Southeast US in summer 2013, with focus on
103 isoprene SOA components and on the relationship between OA and formaldehyde (HCHO).
104 HCHO is a high-yield oxidation product of isoprene (Palmer et al., 2003) and we use the OA-
105 HCHO relationship as a constraint on isoprene SOA yields. SOAS measurements were made at a
106 ground site in rural Centreville, Alabama (Hu et al., 2015; <http://soas2013.rutgers.edu/>).
107 SEAC⁴RS measurements were made from the NASA DC-8 aircraft with extensive boundary
108 layer coverage across the Southeast (Toon et al., 2016; SEAC⁴RS Archive).

109

110 **2. Chemical mechanism for isoprene SOA formation**

111 The default treatment of isoprene SOA in GEOS-Chem at the time of this work (v9-02;
112 <http://geos-chem.org>) followed a standard parameterization operating independently from the
113 gas-phase chemistry mechanism and based on reversible partitioning onto pre-existing OA of
114 generic semivolatile products of isoprene oxidation by OH and NO₃ radicals (Pye et al., 2010).
115 Here we implement a new mechanism for reactive uptake by aqueous aerosols of species
116 produced in the isoprene oxidation cascade of the GEOS-Chem gas-phase mechanism. This
117 couples SOA formation to the gas-phase chemistry and is in accord with increased evidence for a
118 major role of aqueous aerosols in isoprene SOA formation (Ervens et al., 2011).

119 The standard gas-phase isoprene oxidation mechanism in GEOS-Chem v9-02 is
120 described in Mao et al. (2013) and is based on best knowledge at the time building on
121 mechanisms for the oxidation of isoprene by OH (Paulot et al., 2009a; 2009b) and NO₃ (Rollins
122 et al., 2009). Updates implemented in this work are described below and in companion papers
123 applying GEOS-Chem to simulation of observed gas-phase isoprene oxidation products over the
124 Southeast US in summer 2013 (Fisher et al., 2016; Travis et al., 2016). Most gas-phase products
125 of the isoprene oxidation cascade in GEOS-Chem have high dry deposition velocity, competing
126 in some cases with removal by oxidation and aerosol formation (Nguyen et al., 2015a; Travis et
127 al., 2016).

128 Figure 2 shows the isoprene oxidation cascade in GEOS-Chem leading to SOA
129 formation. Reaction pathways leading to isoprene SOA precursors are described below. Yields
130 are in mass percent, unless stated otherwise. Reactive ISOPO₂ isomers formed in the first OH
131 oxidation step react with NO, the hydroperoxyl radical (HO₂), other peroxy radicals (RO₂), or
132 undergo isomerization (Peeters et al., 2009). The NO reaction pathway (high-NO_x pathway)
133 yields C₅ hydroxy carbonyls, methyl vinyl ketone, methacrolein, and first-generation isoprene
134 nitrates (ISOPN). The first three products go on to produce glyoxal and methylglyoxal, which
135 serve as SOA precursors. The overall yield of glyoxal from the high-NO_x pathway is 7 mol %
136 (yield on a molar basis). Oxidation of ISOPN by OH and O₃ is as described by Lee et al. (2014).
137 Reaction of ISOPN with OH produces saturated dihydroxy dinitrates (DHDN), 21 and 27 mol %
138 from the beta and delta channels respectively (Lee et al., 2014), and 10 mol % isoprene
139 epoxydiols (IEPOX) from each channel (Jacobs et al., 2014). We also adopt the mechanism of
140 Lin et al. (2013) to generate C₄ hydroxyepoxides (methacrylic acid epoxide and
141 hydroxymethylmethyl- α -lactone, both denoted MEPOX) from OH oxidation of a

142 peroxyacynitrate formed when methacrolein reacts with OH followed by NO₂. Only
143 hydroxymethylmethyl- α -lactone is shown in Fig. 2.

144 The HO₂ reaction pathway for ISOPO₂ leads to formation of hydroxyhydroperoxides
145 (ISOPOOH) that are oxidized to IEPOX (Paulot et al., 2009b) and several low-volatility
146 products, represented here as C₅-LVOC (Krechmer et al., 2015). The kinetics of IEPOX
147 oxidation by OH is uncertain, and experimentally determined IEPOX lifetimes vary from 8 to 28
148 h for an OH concentration of 1×10^6 molecules cm⁻³ (Jacobs et al., 2013; Bates et al., 2014). In
149 GEOS-Chem we apply the fast kinetics of Jacobs et al. (2013) and reduce the yield of IEPOX
150 from ISOPOOH from 100 to 75%, within the range observed by St. Clair et al. (2016), to address
151 a factor of 4 overestimate in simulated IEPOX (Nguyen et al., 2015a). IEPOX oxidizes to form
152 glyoxal and methylglyoxal (Bates et al., 2014). The overall glyoxal yield from the ISOPO₂ +
153 HO₂ pathway is 6 mol %. Krechmer et al. (2015) report a 2.5 mol % yield of C₅-LVOC from
154 ISOPOOH but we reduce this to 0.5 mol % to reproduce surface observations of the
155 corresponding aerosol products (Section 4). Methyl vinyl ketone and methacrolein yields from
156 the ISOPO₂ + HO₂ pathway are 2.5 and 3.8 mol %, respectively (Liu et al., 2013), sufficiently
157 low that they do not lead to significant SOA formation.

158 Minor channels for ISOPO₂ are isomerization and reaction with RO₂. Isomerization
159 forms hydroperoxyaldehydes (HPALD) that go on to photolyze, but products are uncertain
160 (Peeters and Müller, 2010). We assume 25 mol % yield each of glyoxal and methylglyoxal from
161 HPALD photolysis in GEOS-Chem following Stavrou et al. (2010). Reaction of ISOPO₂ with
162 RO₂ leads to the same suite of C₄-C₅ carbonyls as reaction with NO (C₅ hydroxy carbonyls,
163 methacrolein, and methyl vinyl ketone) and from there to glyoxal and methylglyoxal.

164 Immediate aerosol precursors from the isoprene + OH oxidation cascade are identified in
165 Fig. 2. For the high-NO_x pathway (ISOPO₂ + NO channel) these include glyoxal and
166 methylglyoxal (McNeill et al., 2012), ISOPN (Darer et al., 2011; Hu et al., 2011), DHDN (Lee et
167 al., 2014), MEPOX (Lin et al., 2013), and IEPOX (Jacobs et al., 2014). For the low-NO_x
168 pathway (ISOPO₂ + HO₂ channel) aerosol precursors are IEPOX (Eddingsaas et al., 2010), C₅-
169 LVOC (Krechmer et al., 2015, in which the aerosol-phase species is denoted ISOPOOH-SOA),
170 glyoxal, and methylglyoxal. Glyoxal and methylglyoxal are also produced from the ISOPO₂ +
171 RO₂ and ISOPO₂ isomerization channels.

172 Ozonolysis and oxidation by NO₃ are additional minor isoprene reaction pathways (Fig.
173 2). The NO₃ oxidation pathway is a potentially important source of isoprene SOA at night
174 (Brown et al., 2009) from the irreversible uptake of low-volatility second-generation
175 hydroxynitrates (NT-ISOPN) (Ng et al., 2008; Rollins et al., 2009). We update the gas-phase
176 chemistry of Rollins et al. (2009) as implemented by Mao et al. (2013) to include formation of 4
177 mol % of the aerosol-phase precursor NT-ISOPN from first-generation alkylnitrates (Rollins et
178 al., 2009). Ozonolysis products are volatile and observed SOA yields in chamber studies are low
179 (< 1%; Kleindienst et al., 2007). In GEOS-Chem only methylglyoxal is an aerosol precursor
180 from isoprene ozonolysis.

181 We implement uptake of isoprene oxidation products to aqueous aerosols using
182 laboratory-derived reactive uptake coefficients (γ) as given by Anttila et al. (2006) and Gaston et
183 al. (2014):

184

$$185 \quad \gamma = \left[\frac{1}{\alpha} + \frac{3\omega}{4rRTH^*k_{aq}} \right]^{-1} \quad (1).$$

186

187 Here α is the mass accommodation coefficient (taken as 0.1 for all immediate SOA precursors in
188 Fig. 2), ω is the mean gas-phase molecular speed (cm s⁻¹), r is the aqueous particle radius (cm), R
189 is the universal gas constant (0.08206 L atm K⁻¹ mol⁻¹), T is temperature (K), H^* is the effective
190 Henry's Law constant (M atm⁻¹) accounting for any fast dissociation equilibria in the aqueous
191 phase, and k_{aq} is the pseudo first-order aqueous-phase reaction rate constant (s⁻¹) for conversion
192 to non-volatile products.

193 Precursors with epoxide functionality, IEPOX and MEPOX, undergo acid-catalyzed
194 epoxide ring opening and nucleophilic addition in the aqueous phase. The aqueous-phase rate
195 constant formulation is from Eddingsaas et al. (2010),

$$197 \quad k_{aq} = k_{H^+} [H^+] + k_{nuc} [nuc] [H^+] + k_{HSO_4^-} [HSO_4^-] \quad (2),$$

198
199 and includes three channels: acid-catalyzed ring opening followed by nucleophilic addition of
200 H₂O (k_{H^+} in M⁻¹ s⁻¹) leading to methyltetrols, acid-catalyzed ring opening followed by
201 nucleophilic addition of sulfate and nitrate ions ($nuc \equiv SO_4^{2-} + NO_3^-$, k_{nuc} in M⁻² s⁻¹) leading to
202 organosulfates and organonitrates, and concerted protonation and nucleophilic addition by
203 bisulfate, HSO₄⁻ ($k_{HSO_4^-}$ in M⁻¹ s⁻¹), leading to organosulfates.

204 Precursors with nitrate functionality (-ONO₂), ISOPN and DHDN, hydrolyze to form
205 low-volatility polyols and nitric acid (Hu et al., 2011; Jacobs et al., 2014), so k_{aq} in Eq. (1) is the
206 hydrolysis rate constant.

207 Glyoxal and methylglyoxal form SOA irreversibly by surface uptake followed by
208 aqueous-phase oxidation and oligomerization to yield non-volatile products (Liggio et al., 2005;
209 Volkamer et al., 2009; Nozière et al., 2009; Ervens et al., 2011; Knote et al., 2014). Glyoxal

210 forms SOA with higher yields during the day than at night due to OH aqueous-phase chemistry
211 (Tan et al., 2009; Volkamer et al., 2009; Summer et al., 2014). We use a daytime γ of 2.9×10^{-3}
212 for glyoxal from Liggiio et al. (2005) and a nighttime γ of 5×10^{-6} (Waxman et al., 2013; Sumner
213 et al., 2014). The SOA yield of methylglyoxal is small compared with that of glyoxal (McNeill et
214 al., 2012). A previous GEOS-Chem study by Fu et al. (2008) used the same γ (2.9×10^{-3}) for
215 glyoxal and methylglyoxal. Reaction rate constants are similar for aqueous-phase processing of
216 glyoxal and methylglyoxal (Buxton et al., 1997; Ervens et al., 2003), but H^* of glyoxal is about 4
217 orders of magnitude higher. Here we scale the γ for methylglyoxal to the ratio of effective
218 Henry's law constants: $H^* = 3.7 \times 10^3 \text{ M atm}^{-1}$ for methylglyoxal (Tan et al., 2010) and $H^* = 2.7$
219 $\times 10^7 \text{ M atm}^{-1}$ for glyoxal (Sumner et al., 2014). The resulting uptake of methylglyoxal is very
220 slow and makes a negligible contribution to isoprene SOA.

221 The species C_5 -LVOC from ISOPOOH oxidation and NT-ISOPN from isoprene reaction
222 with NO_3 have very low volatility and are assumed to condense to aerosols with a γ of 0.1
223 limited by mass accommodation. Results are insensitive to the precise value of γ since uptake by
224 aerosols is the main sink for these species in any case.

225 Table 1 gives input variables used to calculate γ for IEPOX, ISOPN, and DHDN by Eqs.
226 (1) and (2). Rate constants are from experiments in concentrated media, representative of
227 aqueous aerosols, so no activity correction factors are applied. Reported experimental values of
228 k_{H^+} vary by an order of magnitude from $1.2 \times 10^{-3} \text{ M}^{-1} \text{ s}^{-1}$ (Eddingsaas et al., 2010) to 3.6×10^{-2}
229 $\text{M}^{-1} \text{ s}^{-1}$ (Cole-Filipiak et al., 2010). Values of k_{nuc} vary by 3 orders of magnitude from $2 \times 10^{-4} \text{ M}^{-2}$
230 s^{-1} (Eddingsaas et al., 2010) to $5.2 \times 10^{-1} \text{ M}^{-2} \text{ s}^{-1}$ (Piletic et al., 2013). We chose values of k_{H^+}
231 and k_{nuc} to fit the SOAS and SEAC⁴RS observations of total IEPOX SOA and IEPOX
232 organosulfates, as shown in Section 4.

233 Table 2 lists average values of γ for all immediate aerosol precursors in the Southeast US
234 boundary layer in summer as simulated by GEOS-Chem (Section 3). γ for IEPOX is a strong
235 function of pH and increases from 1×10^{-4} to 1×10^{-2} as pH decreases from 3 to 0. The value of
236 γ for MEPOX is assumed to be 30 times lower than that of IEPOX when the aerosol is acidic
237 (pH < 4), due to slower acid-catalyzed ring opening (Piletic et al., 2013; Riedel et al., 2015). At
238 pH > 4 we assume that γ for IEPOX and MEPOX are the same (Riedel et al., 2015), but they are
239 then very low.

240 Isoprene SOA formation in clouds is not considered here. Acid-catalyzed pathways
241 would be slow. Observations show that the isoprene SOA yield in the presence of laboratory-
242 generated clouds is low (0.2-0.4%; Brégonzio-Rozier et al., 2015). Wagner et al. (2015) found no
243 significant production of SOA in boundary layer clouds over the Southeast US during SEAC⁴RS.

244

245 3. GEOS-Chem simulation and isoprene SOA yields

246 Several companion papers apply GEOS-Chem to interpret SEAC⁴RS and surface data
247 over the Southeast US in summer 2013 including Kim et al. (2015) for aerosols, Fisher et al.
248 (2016) for organic nitrates, Travis et al. (2016) for ozone and NO_x, and Zhu et al. (2016) for
249 HCHO. These studies use a model version with $0.25^\circ \times 0.3125^\circ$ horizontal resolution over North
250 America, nested within a $4^\circ \times 5^\circ$ global simulation. Here we use a $2^\circ \times 2.5^\circ$ global GEOS-Chem
251 simulation with no nesting. Yu et al. (2016) found little difference between $0.25^\circ \times 0.3125^\circ$ and
252 $2^\circ \times 2.5^\circ$ resolutions in simulated regional statistics for isoprene chemistry.

253 The reader is referred to Kim et al. (2015) for a general presentation of the model, the
254 treatment of aerosol sources and sinks, and evaluation with Southeast US aerosol observations;
255 and to Travis et al. (2016) and Fisher et al. (2016) for presentation of gas-phase chemistry and

256 comparisons with observed gas-phase isoprene oxidation products. Isoprene emission is from the
257 MEGAN v2.1 inventory (Guenther et al., 2012). The companion papers decrease isoprene
258 emission by 15% from the MEGAN v2.1 values to fit the HCHO data (Zhu et al., 2016), but this
259 is not applied here.

260 Our SOA simulation differs from that of Kim et al. (2015). They assumed fixed 3% and
261 10% mass yields of SOA from isoprene and monoterpenes, respectively, and parameterized SOA
262 formation from anthropogenic and open fire sources as a kinetic irreversible process following
263 Hodzic and Jimenez (2011). Here we use our new aqueous-phase mechanism for isoprene SOA
264 coupled to gas-phase chemistry as described in Section 2, and otherwise use the semivolatile
265 reversible partitioning scheme of Pye et al. (2010) for monoterpene, anthropogenic, and open fire
266 SOA. Kim et al. (2015) found no systematic bias in detailed comparisons to OA measurements
267 from SEAC⁴RS and from surface networks. We find a low bias, as shown below, because the
268 reversible partitioning scheme yields low SOA concentrations.

269 Organic aerosol and sulfate contribute most of the aerosol mass over the Southeast US in
270 summer, while nitrate is negligibly small (Kim et al., 2015). GEOS-Chem uses the ISORROPIA
271 thermodynamic model (Fountoukis and Nenes, 2007) to simulate sulfate-nitrate-ammonium
272 (SNA) aerosol composition, water content, and acidity as a function of local conditions.
273 Simulated aerosol pH along the SEAC⁴RS flight tracks in the Southeast US boundary layer
274 averages 1.3 (interquartiles 0.92 and 1.8). The aerosol pH remains below 3 even when sulfate
275 aerosol is fully neutralized by ammonia (Guo et al., 2015).

276 We consider that the aqueous aerosol population where isoprene SOA formation can take
277 place is defined by the sulfate aerosol population. This assumes that all aqueous aerosol particles
278 contain some sulfate, and that all sulfate is aqueous. Clear-sky RH measured from the aircraft in

279 the Southeast US boundary layer during SEAC⁴RS averaged $72 \pm 17\%$, and the corresponding
280 values in GEOS-Chem sampled along the flight tracks averaged $66 \pm 16\%$. These RHs are
281 sufficiently high that sulfate aerosol can reliably be expected to be aqueous (Wang et al., 2008).
282 The rate of gas uptake by the sulfate aerosol is computed with the pseudo-first order reaction rate
283 constant k_{het} (s^{-1}) (Schwartz, 1986; Jacob, 2000):

284

$$285 \quad k_{het} = \int_0^{\infty} 4\pi r^2 \left(\frac{r}{D_g} + \frac{4}{\gamma\omega} \right)^{-1} n(r) dr \quad (3),$$

286

287 where D_g is the gas-phase diffusion constant (taken to be $0.1 \text{ cm}^2 \text{ s}^{-1}$) and $n(r)$ is the number size
288 distribution of sulfate aerosol (cm^{-4}). The first and second terms in parentheses describe the
289 limitations to gas uptake from gas-phase diffusion and aqueous-phase reaction, respectively.

290 The sulfate aerosol size distribution including RH-dependent hygroscopic growth factors
291 is from the Global Aerosol Data Set (GADS) of Koepke et al. (1997), as originally implemented
292 in GEOS-Chem by Martin et al. (2003) and updated by Drury et al. (2010). The GADS size
293 distribution compares well with observations over the eastern US in summer (Drury et al., 2010),
294 including for SEAC⁴RS (Kim et al., 2015). We compute $n(r)$ locally in GEOS-Chem by taking
295 the dry SNA mass concentration, converting from mass to volume with a dry aerosol mass
296 density of 1700 kg m^{-3} (Hess et al., 1998), applying the aerosol volume to the dry sulfate size
297 distribution in GADS, and then applying the GADS hygroscopic growth factors. We verified that
298 the hygroscopic growth factors from GADS agree within 10% with those computed locally from
299 ISORROPIA.

300 Figure 2 shows the mean branching ratios for isoprene oxidation in the Southeast US
301 boundary layer as calculated by GEOS-Chem. 87% of isoprene reacts with OH, 8% with ozone,
302 and 5% with NO_3 . Oxidation of isoprene by OH produces ISOPO_2 of which 51% reacts with NO
303 (high- NO_x pathway), 35% reacts with HO_2 , 8% isomerizes, and 6% reacts with other RO_2
304 radicals.

305 Glyoxal is an aerosol precursor common to all isoprene + OH pathways in our
306 mechanism with yields of 7 mol % from the $\text{ISOPO}_2 + \text{NO}$ pathway, 6 mol % from $\text{ISOPO}_2 +$
307 HO_2 , 11 mol % from $\text{ISOPO}_2 + \text{RO}_2$, and 25 mol % from ISOPO_2 isomerization. For the
308 Southeast US conditions we thus find that 44% of glyoxal is from the $\text{ISOPO}_2 + \text{NO}$ pathway,
309 24% from $\text{ISOPO}_2 + \text{HO}_2$, 8% from $\text{ISOPO}_2 + \text{RO}_2$, and 24% from ISOPO_2 isomerization.

310 The mean total yield of isoprene SOA computed in GEOS-Chem for the Southeast US
311 boundary layer is 3.3%, as shown in Fig. 2. IEPOX contributes 1.9% and glyoxal 0.9%. The low-
312 NO_x pathway involving ISOPO_2 reaction with HO_2 contributes 73% of the total isoprene SOA
313 yield, mostly from IEPOX, even though this pathway is only 35% of the fate of ISOPO_2 . The
314 high- NO_x pathway contributes 16% of isoprene SOA, mostly from glyoxal. MEPOX
315 contribution to isoprene SOA is small (2%) and consistent with a recent laboratory study that
316 finds low SOA yields from this pathway under humid conditions (Nguyen et al., 2015b). The
317 minor low- NO_x pathways from ISOPO_2 isomerization and reaction with RO_2 contribute 8% of
318 isoprene SOA through glyoxal. The remainder of isoprene SOA formation (3%) is from
319 nighttime oxidation by NO_3 .

320 The dominance of IEPOX and glyoxal as precursors for isoprene SOA was previously
321 found by McNeill et al. (2012) using a photochemical box model. Both IEPOX and glyoxal are
322 produced photochemically, and both are removed photochemically in the gas phase by reaction

323 with OH (and photolysis for glyoxal). The mean lifetimes of IEPOX and glyoxal against gas-
324 phase photochemical loss average 1.6 and 2.3 h respectively for SEAC⁴RS daytime conditions;
325 mean lifetimes against reactive uptake by aerosol are 31 and 20 hours, respectively. For both
326 species, aerosol uptake is thus a minor sink competing with gas-phase photochemical loss. The
327 model yield of IEPOX SOA from IEPOX is 5% in the boundary layer, consistent with average
328 yields from chamber experiments (4-10%) for aerosols with similar acidity to aerosols in the
329 Southeast US (Riedel et al., 2015).

330 The dominance of gas-phase loss over aerosol uptake for both IEPOX and glyoxal
331 implies that isoprene SOA formation is highly sensitive to their reactive uptake coefficients γ and
332 to the aqueous aerosol mass concentration (in both cases, γ is small enough that uptake is
333 controlled by bulk aqueous-phase rather than surface reactions). We find under SEAC⁴RS
334 conditions that γ for IEPOX is mainly controlled by the H^+ concentration ($k_{H^+}[H^+]$ in Eq. (2)),
335 with little contribution from nucleophile-driven and HSO_4^- -driven channels. This will be
336 discussed below in comparison to SOAS and SEAC⁴RS observations.

337 The 3.3% mean yield of isoprene SOA from our mechanism is consistent with the fixed
338 yield of 3% assumed by Kim et al. (2015) in their GEOS-Chem simulation of the SEAC⁴RS
339 period, including extensive comparisons to OA observations that showed a 40% mean
340 contribution of isoprene to total OA. We conducted a sensitivity simulation using the default
341 isoprene SOA mechanism in GEOS-Chem based on reversible partitioning of semivolatile
342 oxidation products onto pre-existing OA (Pye et al., 2010). The isoprene SOA yield in that
343 simulation was only 1.1%. The observed correlation of OA with HCHO in SEAC⁴RS supports
344 our higher yield, as shown below.

345

346 4. Observational constraints on isoprene SOA yields

347 Isoprene is the largest source of HCHO in the Southeast US (Millet et al., 2006), and we
348 use the observed relationship between OA and HCHO to evaluate the GEOS-Chem isoprene
349 SOA yields. The SEAC⁴RS aircraft payload included measurements of OA from an Aerodyne
350 Aerosol Mass Spectrometer (HR-ToF-AMS; DeCarlo et al, 2006; Canagaratna et al, 2007)
351 concurrent with HCHO from a laser-induced fluorescence instrument (ISAF; Cazorla et al.,
352 2015). Column HCHO was also measured during SEAC⁴RS from the OMI satellite instrument
353 (González Abad et al., 2015; Zhu et al., 2016), providing a proxy for isoprene emission (Palmer
354 et al., 2003; 2006).

355 Figure 3 (left) shows the observed and simulated relationships between OA and HCHO
356 mixing ratios in the boundary layer. There is a strong correlation in the observations and in the
357 model ($R = 0.79$ and $R = 0.82$, respectively). OA simulated with our aqueous-phase isoprene
358 SOA mechanism reproduces the observed slope ($2.8 \pm 0.3 \mu\text{g sm}^{-3} \text{ ppbv}^{-1}$, vs. $3.0 \pm 0.4 \mu\text{g sm}^{-3}$
359 ppbv^{-1} in the observations). Similarly strong correlations and consistency between model and
360 observations are found with column HCHO measured from OMI (Fig. 3, right). The estimated
361 error on individual OMI HCHO observations is about 30% (Millet et al., 2006).

362 Also shown in Fig. 3 is a sensitivity simulation with the default GEOS-Chem mechanism
363 based on reversible partitioning with pre-existing organic aerosol (Pye et al., 2010) and
364 producing a 1.1% mean isoprene SOA yield, as compared to 3.3% in our simulation with the
365 aqueous-phase mechanism. That sensitivity simulation shows the same OA-HCHO correlation
366 ($R = 0.82$) but underestimates the slope ($2.0 \pm 0.3 \mu\text{g sm}^{-3} \text{ ppbv}^{-1}$). The factor of 3 increase in our
367 isoprene SOA yield does not induce a proportional increase in the slope, as isoprene contributes
368 only $\sim 40\%$ of OA in the Southeast US. But the slope is sensitive to the isoprene SOA yield, and

369 the good agreement between our simulation and observations supports our estimate of a mean
370 3.3% yield for the Southeast US.

371 Figure 3 shows an offset between the model and observations illustrated by the regression
372 lines. We overestimate HCHO by 0.4 ppbv on average because we did not apply the 15%
373 downward correction to MEGAN v2.1 isoprene emissions (Zhu et al., 2016). We also
374 underestimate total OA measured by the AMS in the boundary layer by $1.1 \mu\text{g sm}^{-3}$ (mean AMS
375 OA is $5.8 \pm 4.3 \mu\text{g sm}^{-3}$; model OA is $4.7 \pm 4.4 \mu\text{g sm}^{-3}$). The bias can be explained by our
376 omission of anthropogenic and open fire SOA, found by Kim et al. (2015) to account on average
377 for 18% of OA in SEAC⁴RS.

378 Figure 4 shows time series of the isoprene SOA components IEPOX SOA and C₅-LVOC
379 SOA at Centreville, Alabama during SOAS. AMS observations from Hu et al. (2015) and
380 Krechmer et al. (2015) are compared to model values. IEPOX SOA and C₅-LVOC SOA are on
381 average 17% and 2% of total AMS OA, respectively (Hu et al., 2015; Krechmer et al., 2015).
382 The model reproduces mean IEPOX SOA and C₅-LVOC SOA without bias, supporting the
383 conclusion that IEPOX is the dominant contributor to isoprene SOA in the Southeast US (Fig. 2).
384 Low values on July 2-7, both in the observations and the model, are due to low temperatures
385 suppressing isoprene emission.

386 Figure 5 shows the relationships of daily mean IEPOX SOA and sulfate concentrations at
387 Centreville and in the SEAC⁴RS boundary layer. The same factor analysis method was used to
388 derive IEPOX SOA in SEAC⁴RS as in SOAS, however the uncertainty is larger for the aircraft
389 observations due to the much wider range of conditions encountered. There is a strong
390 correlation between IEPOX SOA and sulfate, both in observations and the model, with similar
391 slopes. Correlation between IEPOX SOA and sulfate has similarly been observed at numerous

392 Southeast US monitoring sites (Budisulistiorini et al., 2013; 2015; Xu et al., 2015; Hu et al.,
393 2015). Xu et al. (2015) concluded that IEPOX SOA must form by acid-catalyzed nucleophilic
394 addition of sulfate (sulfate channels in Eq. (2)) leading to organosulfates. However, we find in
395 our model that the H^+ -catalyzed channel ($k_{H^+}[H^+]$ term in Eq. (2)) contributes 90% of IEPOX
396 SOA formation throughout the Southeast US boundary layer, and that sulfate channels play only
397 a minor role. Thus the correlation of IEPOX SOA and sulfate is not an indication of
398 organosulfate formation but rather reflects the correlation of sulfate with aqueous aerosol volume
399 and acidity. Measurements from the PALMS laser mass spectrometer during SEAC⁴RS (Liao et
400 al., 2015) show a mean IEPOX organosulfate concentration of $0.13 \mu\text{g sm}^{-3}$, amounting to at
401 most 9% of total IEPOX SOA. The organosulfate should be a marker of the sulfate channels
402 because its hydrolysis is negligibly slow (Hu et al., 2011).

403 Formation of IEPOX SOA is nearly linear with k_{het} in Eq. (3) as aqueous aerosol is only a
404 minor sink for IEPOX. IEPOX γ is sufficiently small (Table 2) that gas-phase diffusion and mass
405 accommodation are not limiting processes. k_{aq} in Eq. (2) is dominated by the $k_{H^+}[H^+]$ term as
406 discussed above. It follows from combination of Eqs. (1), (2), and (3) that IEPOX SOA
407 formation is proportional to $V[H^+]$, where V is the volume concentration of aqueous aerosol. An
408 increased supply of sulfate as sulfuric acid increases both V and $[H^+]$, explaining the correlation
409 between IEPOX SOA and sulfate.

410 Correlation between IEPOX SOA and sulfate is also apparent in the spatial distribution of
411 IEPOX SOA, as observed by the SEAC⁴RS aircraft below 2 km and simulated by GEOS-Chem
412 along the aircraft flight tracks (Fig. 6). The correlation between simulated and observed IEPOX
413 SOA in Fig. 6 is $R = 0.70$. Average (mean) IEPOX SOA is $1.4 \pm 1.4 \mu\text{g sm}^{-3}$ in the observations
414 and $1.3 \pm 1.2 \mu\text{g sm}^{-3}$ in the model. The correlation between IEPOX SOA and sulfate is 0.66 in

415 the observations and 0.77 in the model. IEPOX SOA concentrations are highest in the industrial
416 Midwest and Kentucky, and in Louisiana-Mississippi, coincident with the highest sulfate
417 concentrations sampled on the flights. We also see in Fig. 6 frequent observations of very low
418 IEPOX SOA (less than $0.4 \mu\text{g sm}^{-3}$) that are well captured by the model. These are associated
419 with very low sulfate (less than $1 \mu\text{g sm}^{-3}$).

420 The mean IEPOX SOA concentration simulated by the model for the SEAC⁴RS period
421 (background contours in Fig. 6) is far more uniform than IEPOX SOA simulated along the flight
422 tracks. This shows the importance of day-to-day variations in sulfate in driving IEPOX SOA
423 variability. IEPOX SOA contributed on average 24% of total OA in the SEAC⁴RS observations,
424 and 28% in GEOS-Chem sampled along the flight tracks and as a regional mean. With IEPOX
425 SOA accounting for 58% of isoprene SOA in the model (Fig. 2), this amounts to a 41-48%
426 contribution of isoprene to total OA, consistent with the previous estimate of 40% by Kim et al.
427 (2015).

428

429 **5. Effect of Anthropogenic Emission Reductions**

430 The EPA projects that US anthropogenic emissions of NO_x and SO_2 will decrease
431 respectively by 34% and 48% from 2013 to 2025 (EPA, 2014). We conducted a GEOS-Chem
432 sensitivity simulation to examine the effect of these changes on isoprene SOA, assuming no
433 other changes and further assuming that the emission decreases are uniform across the US.

434 Figure 7 shows the individual and combined effects of NO_x and SO_2 emission reductions
435 on the branching pathways for isoprene oxidation, sulfate mass concentration, aerosol pH, and
436 isoprene SOA in the Southeast US boundary layer in summer. Reducing NO_x emission by 34%
437 decreases the mean NO concentration by only 23%, in part because decreasing OH increases the

438 NO_x lifetime and in part because decreasing ozone increases the NO/NO₂ ratio. There is no
439 change in HO₂. We find a 10% decrease in the high-NO_x pathway and a 6% increase in the low-
440 NO_x pathway involving ISOP₂O₂ + HO₂. Aerosol sulfate decreases by 2% and there is no change
441 in [H⁺]. The net effect is a 7% increase in isoprene SOA, as the major individual components
442 IEPOX SOA and glyoxal SOA increase by 17% and decrease by 8%, respectively.

443 A 48% decrease in SO₂ emissions drives a 36% reduction in sulfate mass concentration,
444 leading to a decline in aerosol volume (31%) that reduces uptake of all isoprene SOA precursors.
445 The decrease in aerosol [H⁺] (26%) further reduces IEPOX uptake. Decline in aerosol volume
446 and [H⁺] have a comparable effect on IEPOX SOA, as the change in each due to SO₂ emission
447 reductions is similar (~30%) and uptake of IEPOX SOA is proportional to the product of the two
448 (Section 4). IEPOX SOA and glyoxal SOA decrease by 45% and 26%, respectively, and total
449 isoprene SOA decreases by 35%. Pye et al. (2013) included uptake of IEPOX to aqueous
450 aerosols in a regional chemical transport model and similarly found that SO₂ emissions are more
451 effective than NO_x emissions at reducing IEPOX SOA in the Southeast US. Remarkably, we find
452 that reducing SO₂ emissions decreases sulfate and isoprene SOA with similar effectiveness (Fig.
453 7). With sulfate contributing ~30% of present-day PM_{2.5} in the Southeast US and isoprene SOA
454 contributing ~25% (Kim et al., 2015), this represents a factor of 2 co-benefit on PM_{2.5} from
455 reducing SO₂ emissions.

456 We examined whether this co-benefit from reducing SO₂ emissions can be seen in past
457 decadal trends. Observations from monitoring networks in the Southeast US show that
458 summertime OA and sulfate concentrations declined from 2003 to 2013 at rates of 3.9% a⁻¹ and
459 7.4% a⁻¹, respectively, while wintertime OA showed no significant decrease (Kim et al., 2015).
460 With isoprene accounting for 40% of OA in summer (Kim et al., 2015), and assuming no trend in

461 other OA components on the basis of the wintertime data, we would infer a rate of isoprene SOA
462 decrease of 9.8% a⁻¹. The observed trends thus seem to support a similar relative rate of decrease
463 of sulfate and isoprene SOA over the past decade.

464

465 **6. Conclusions**

466 Standard mechanisms for formation of isoprene secondary organic aerosol (SOA) in
467 chemical transport models assume reversible partitioning of isoprene oxidation products to pre-
468 existing dry OA. This may be appropriate for dry conditions in experimental chambers but not
469 for typical atmospheric conditions where the aerosol is mostly aqueous. Here we developed an
470 aqueous-phase reactive uptake mechanism coupled to a detailed gas-phase isoprene chemistry
471 mechanism to describe the reactive uptake of water-soluble isoprene oxidation products to
472 aqueous aerosol. We applied this mechanism in the GEOS-Chem chemical transport model to
473 simulate surface (SOAS) and aircraft (SEAC⁴RS) observations over the Southeast US in summer
474 2013.

475 Our mechanism includes different channels for isoprene SOA formation by the high-NO_x
476 pathway, when the isoprene peroxy radicals (ISOPO₂) react with NO, and in the low-NO_x
477 pathway where they react mostly with HO₂. The main SOA precursors are found to be isoprene
478 epoxide (IEPOX) in the low-NO_x pathway and glyoxal in the high- and low-NO_x pathways. Both
479 of these precursors have dominant gas-phase photochemical sinks, and so their uptake by
480 aqueous aerosol is nearly proportional to the reactive uptake coefficient γ and to the aqueous
481 aerosol mass concentration. The γ for IEPOX is mostly determined by the rate of H⁺-catalyzed
482 ring opening in the aqueous phase.

483 Application of our mechanism to the Southeast US indicates a mean isoprene SOA yield
484 of 3.3% on a mass basis. By contrast, a conventional mechanism based on reversible uptake of
485 semivolatile isoprene oxidation products yields only 1.1%. Simulation of the observed
486 relationship of OA with formaldehyde (HCHO) provides support for our higher yield. We find
487 that the low-NO_x pathway is 5 times more efficient than the high-NO_x pathway for isoprene SOA
488 production. Under Southeast US conditions, IEPOX and glyoxal account respectively for 58%
489 and 28% of isoprene SOA.

490 Our model simulates well the observations and variability of IEPOX SOA at the surface
491 and from aircraft. The observations show a strong correlation with sulfate that we reproduce in
492 the model. This correlation was previously attributed to acid-catalyzed nucleophilic addition of
493 sulfate as mechanism for IEPOX SOA formation but we find in the model that this pathway is
494 minor. We find instead that the correlation of IEPOX SOA with sulfate is due to the effect of
495 sulfate on aerosol pH and volume concentration, increasing IEPOX uptake by the H⁺-catalyzed
496 ring-opening mechanism. Low concentrations of sulfate are associated with very low IEPOX
497 SOA, both in the observations and the model, and we attribute this to the compounding effects of
498 low sulfate on aerosol [H⁺] and on aerosol volume.

499 The US EPA has projected that US NO_x and SO₂ emissions will decrease by 34 and 48%
500 respectively from 2013 to 2025. We find in our model that the NO_x reduction will increase
501 isoprene SOA by 7%, reflecting greater importance of the low-NO_x pathway. The SO₂ reduction
502 will decrease isoprene SOA by 35%, due to decreases in both aerosol [H⁺] and volume
503 concentration. The combined effect of these two changes is to decrease isoprene SOA by 32%,
504 corresponding to a decrease in the isoprene SOA mass yield from 3.3% to 2.3%. Decreasing SO₂
505 emissions by 48% has similar relative effects on sulfate (36%) and isoprene SOA (35%).

506 Considering that sulfate presently accounts for about 30% of PM_{2.5} in the Southeast US in
507 summer, while isoprene SOA contributes 25%, we conclude that decreasing isoprene SOA
508 represents a factor of 2 co-benefit when reducing SO₂ emissions. There is some evidence for this
509 co-benefit in observed long-term trends of OA in the Southeast US over the past decade.

510

511 **Acknowledgements**

512 We are grateful to the entire NASA SEAC⁴RS team for their help in the field, in
513 particular Paul Wennberg, John Crouse, Jason St. Clair, and Alex Teng for their CIT-CIMS
514 measurements. Thanks also to Jesse Kroll for assisting in the interpretation of chamber study
515 results. This work was funded by the NASA Tropospheric Chemistry Program, the NASA Air
516 Quality Applied Sciences Team, and a South African National Research Foundation Fellowship
517 and Schlumberger Faculty for the Future Fellowship to EAM. WH, JEK, PCJ, DAD, and JLJ
518 were supported by NASA NNX12AC03G/NNX15AT96G and NSF AGS-1243354. JEK was
519 supported by EPA STAR (FP-91770901-0) and CIRES Fellowships. JAF acknowledges support
520 from a University of Wollongong Vice Chancellor's Postdoctoral Fellowship. HCHO
521 observations were acquired with support from NASA ROSES SEAC⁴RS grant
522 NNH10ZDA001N. Although this document has been reviewed by U.S. EPA and approved for
523 publication, it does not necessarily reflect U.S. EPA's policies or views.

524

525 **References**

- 526 Anttila, T., Kiendler-Scharr, A., Tillmann, R., and Mentel, T. F.: On the reactive uptake of
527 gaseous compounds by organic-coated aqueous aerosols: Theoretical analysis and
528 application to the heterogeneous hydrolysis of N₂O₅, *J. Phys. Chem. A*, 110, 10435-10443,
529 doi:10.1021/jp062403c, 2006.
- 530 Attwood, A. R., Washenfelder, R. A., Brock, C. A., Hu, W., Baumann, K., Campuzano-Jost, P.,
531 Day, D. A., Edgerton, E. S., Murphy, D. M., Palm, B. B., McComiskey, A., Wagner, N. L.,
532 de Sá, S. S., Ortega, A., Martin, S. T., Jimenez, J. L., and Brown, S. S.: Trends in sulfate
533 and organic aerosol mass in the Southeast U.S.: Impact on aerosol optical depth and
534 radiative forcing, *Geophys. Res. Lett.*, 41, 7701-7709, doi:10.1002/2014gl061669, 2014.
- 535 Bateman, A. P., Bertram, A. K., and Martin, S. T.: Hygroscopic influence on the semisolid-to-
536 liquid transition of secondary organic materials, *J. Phys. Chem. A*, 119, 4386-4395,
537 doi:10.1021/jp508521c, 2014.
- 538 Bates, K. H., Crounse, J. D., St Clair, J. M., Bennett, N. B., Nguyen, T. B., Seinfeld, J. H., Stoltz,
539 B. M., and Wennberg, P. O.: Gas phase production and loss of isoprene epoxydiols, *J.*
540 *Phys. Chem. A*, 118, 1237-1246, doi:10.1021/jp4107958, 2014.
- 541 Brégonzio-Rozier, L., Giorio, C., Siekmann, F., Pangui, E., Morales, S. B., Temime-Roussel, B.,
542 Gratien, A., Michoud, V., Cazaunau, M., DeWitt, H. L., Tapparo, A., Monod, A.,
543 and Doussin, J.-F.: Secondary organic aerosol formation from isoprene photooxidation
544 during cloud condensation–evaporation cycles, *Atmos. Chem. Phys. Discuss.*, 15, 20561-
545 20596, doi:10.5194/acpd-15-20561-2015, 2015.
- 546 Brown, S. S., De Gouw, J. A., Warneke, C., Ryerson, T. B., Dubé, W. P., Atlas, E., Weber, R. J.,
547 Peltier, R. E., Neuman, J. A., Roberts, J. M., Swanson, A., Flocke, F., McKeen, S. A.,
548 Brioude, J., Sommariva, R., Trainer, M., Fehsenfeld, F. C., and Ravishankara, A. R.:
549 Nocturnal isoprene oxidation over the Northeast United States in summer and its impact on
550 reactive nitrogen partitioning and secondary organic aerosol, *Atmos. Chem. Phys.*, 9, 3027-
551 3042, doi:10.5194/acp-9-3027-2009, 2009.
- 552 Budisulistiorini, S. H., Canagaratna, M. R., Croteau, P. L., Marth, W. J., Baumann, K., Edgerton,
553 E. S., Shaw, S. L., Knipping, E. M., Worsnop, D. R., Jayne, J. T., Gold, A., and Surratt, J.
554 D.: Real-time continuous characterization of secondary organic aerosol derived from
555 isoprene epoxydiols in downtown Atlanta, Georgia, using the Aerodyne aerosol chemical
556 speciation monitor, *Environ. Sci. Technol.*, 47, 5686-5694, doi:10.1021/es400023n, 2013.
- 557 Budisulistiorini, S. H., Li, X., Bairai, S. T., Renfro, J., Liu, Y., Liu, Y. J., McKinney, K. A.,
558 Martin, S. T., McNeill, V. F., Pye, H. O. T., Nenes, A., Neff, M. E., Stone, E. A., Mueller,
559 S., Knote, C., Shaw, S. L., Zhang, Z., Gold, A., and Surratt, J. D.: Examining the effects of
560 anthropogenic emissions on isoprene-derived secondary organic aerosol formation during
561 the 2013 Southern Oxidant and Aerosol Study (SOAS) at the Look Rock, Tennessee
562 ground site, *Atmos. Chem. Phys.*, 15, 8871-8888, doi:10.5194/acp-15-8871-2015, 2015.
- 563 Buxton, G. V., Malone, T. N., and Salmon, G. A.: Oxidation of glyoxal initiated by •OH in
564 oxygenated aqueous solution, *J Chem. Soc. Faraday T.*, 93, 2889-2891, doi
565 10.1039/A701468f, 1997.
- 566

- 567 Canagaratna, M. R., Jayne, J. T., Jimenez, J. L., Allan, J. D., Alfarra, M. R., Zhang, Q., Onasch,
568 T. B., Drewnick, F., Coe, H., Middlebrook, A., Delia, A., Williams, L. R., Trimborn, A.
569 M., Northway, M. J., DeCarlo, P. F., Kolb, C. E., Davidovits, P., Worsnop, D. R.:
570 Chemical and microphysical characterization of ambient aerosols with the Aerodyne
571 Aerosol Mass Spectrometer. *Mass Spectrometry Reviews*, 26, 185-222, doi:
572 10.1002/mas.20115, 2007.
- 573 Carlton, A. G., Turpin, B. J., Altieri, K. E., Seitzinger, S. P., Mathur, R., Roselle, S. J., and
574 Weber, R. J.: CMAQ model performance enhanced when in-cloud secondary organic
575 aerosol is included: Comparisons of organic carbon predictions with measurements,
576 *Environ. Sci. Technol.*, 42, 8789–8802, doi:10.1021/es801192n, 2008.
- 577 Carlton, A. G., Wiedinmyer, C., and Kroll, J. H.: A review of secondary organic aerosol (SOA)
578 formation from isoprene, *Atmos. Chem. Phys.*, 9, 4987-5005, doi:10.5194/acp-9-4987-
579 2009, 2009.
- 580 Carlton, A. G., and Turpin, B. J.: Particle partitioning potential of organic compounds is highest
581 in the Eastern US and driven by anthropogenic water, *Atmos. Chem. Phys.*, 13, 10203-
582 10214, doi:10.5194/acp-13-10203-2013, 2013.
- 583 Cazorla, M., Wolfe, G. M., Bailey, S. A., Swanson, A. K., Arkinson, H. L., and Hanisco, T. F.: A
584 new airborne laser-induced fluorescence instrument for in situ detection of formaldehyde
585 throughout the troposphere and lower stratosphere, *Atmos. Meas. Tech.*, 8, 541-552,
586 doi:10.5194/amt-8-541-2015, 2015.
- 587 Chan, A. W. H., Chan, M. N., Surratt, J. D., Chhabra, P. S., Loza, C. L., Crouse, J. D., Yee, L.
588 D., Flagan, R. C., Wennberg, P. O., and Seinfeld, J. H.: Role of aldehyde chemistry and
589 NO_x concentrations in secondary organic aerosol formation, *Atmos. Chem. Phys.*, 10,
590 7169-7188, doi:10.5194/acp-10-7169-2010, 2010.
- 591 Cole-Filipiak, N. C., O'Connor, A. E., and Elrod, M. J.: Kinetics of the hydrolysis of
592 atmospherically relevant isoprene-derived hydroxy epoxides, *Environ. Sci. Technol.*, 44,
593 6718-6723, doi:10.1021/es1019228, 2010.
- 594 Darer, A. I., Cole-Filipiak, N. C., O'Connor, A. E., and Elrod, M. J.: Formation and stability of
595 atmospherically relevant isoprene-derived organosulfates and organonitrates, *Environ. Sci.*
596 *Technol.*, 45, 1895-1902, doi:10.1021/es103797z, 2011.
- 597 DeCarlo, P. F., Kimmel, J. R., Trimborn, A., Northway, M. J., Jayne, J. T., Aiken, A. C., Gonin,
598 M., Fuhrer, K., Horvath, T., Docherty, K. S., Worsnop, D. R., and Jimenez, J. L.: Field-
599 deployable, High-Resolution, Time-of-Flight Aerosol Mass Spectrometer, *Anal. Chem.*, 78,
600 8281-8289, doi: 10.1021/ac061249n, 2006.
- 601 Dommen, J., Metzger, A., Duplissy, J., Kalberer, M., Alfarra, M. R., Gascho, A., Weingartner,
602 E., Prévôt, A. S. H., Verheggen, B., and Baltensperger, U.: Laboratory observation of
603 oligomers in the aerosol from isoprene/NO_x photooxidation, *Geophys. Res. Lett.*, 33,
604 L13805, doi:10.1029/2006gl026523, 2006.
- 605 Donahue, N. M., Robinson, A. L., Stanier, C. O., and Pandis, S. N.: Coupled partitioning,
606 dilution, and chemical aging of semivolatile organics, *Environ. Sci. Technol.*, 40, 2635-
607 2643, doi:10.1021/es052297c, 2006.

608 Drury, E., Jacob, D. J., Spurr, R. J. D., Wang, J., Shinozuka, Y., Anderson, B. E., Clarke, A. D.,
609 Dibb, J., McNaughton, C., and Weber, R.: Synthesis of satellite (MODIS), aircraft
610 (ICARTT), and surface (IMPROVE, EPA-AQS, AERONET) aerosol observations over
611 eastern North America to improve MODIS aerosol retrievals and constrain surface aerosol
612 concentrations and sources, *J. Geophys. Res.*, 115, D14204, doi:10.1029/2009jd012629,
613 2010.

614 EPA: U. S. Environmental Protection Agency, Technical Support Document (TSD): Preparation
615 of Emissions Inventories for the Version 6.1, 2011 Emissions Modeling Platform, available
616 at: [http://www.epa.gov/ttn/chief/emch/2011v6/2011v6.1_2018_2025_base_EmisMod_TSD](http://www.epa.gov/ttn/chief/emch/2011v6/2011v6.1_2018_2025_base_EmisMod_TSD_nov2014_v6.pdf)
617 [_nov2014_v6.pdf](http://www.epa.gov/ttn/chief/emch/2011v6/2011v6.1_2018_2025_base_EmisMod_TSD_nov2014_v6.pdf) (Accessed on July 15, 2015), 2014.

618 Eddingsaas, N. C., VanderVelde, D. G., and Wennberg, P. O.: Kinetics and products of the acid-
619 catalyzed ring-opening of atmospherically relevant butyl epoxy alcohols, *J. Phys. Chem. A*,
620 114, 8106-8113, doi:10.1021/jp103907c, 2010.

621 Edney, E. O., Kleindienst, T. E., Jaoui, M., Lewandowski, M., Offenberg, J. H., Wang, W., and
622 Claeys, M.: Formation of 2-methyl tetrols and 2-methylglyceric acid in secondary organic
623 aerosol from laboratory irradiated isoprene/NO_x/SO₂/air mixtures and their detection in
624 ambient PM_{2.5} samples collected in the eastern United States, *Atmos. Environ.*, 39, 5281-
625 5289, doi:10.1016/j.atmosenv.2005.05.031, 2005.

626 Ervens, B., Gligorovski, S., and Herrmann, H.: Temperature-dependent rate constants for
627 hydroxyl radical reactions with organic compounds in aqueous solutions, *Phys. Chem.*
628 *Chem. Phys.*, 5, 1811-1824, doi:10.1039/b300072a, 2003.

629 Ervens, B., Turpin, B. J., and Weber, R. J.: Secondary organic aerosol formation in cloud
630 droplets and aqueous particles (aqSOA): A review of laboratory, field and model studies,
631 *Atmos. Chem. Phys.*, 11, 11069-11102, doi:10.5194/acp-11-11069-2011, 2011.

632 Fisher, J. A., Jacob, D., Travis, K. R., Kim, P. S., Marais, E. A., Miller, C. C., Yu, K., Zhu, L.,
633 Yantosca, R. M., Sulprizio, M. P., Mao, J., Wennberg, P. O., Crouse, J. D., Teng, A. P.,
634 Nguyen, T. B., Cohen, R. C., Romer, P., Nault, B. A., Jimenez, J. L., Campuzano-Jost, P.,
635 Shepson, P. B., Xiong, F., Blake, D. R., Goldstein, A. H., Hanisco, T. F., Ryerson, T. B.,
636 Wisthaler, A., and Mikoviny, T.: Organic nitrate chemistry and its implications for nitrogen
637 budgets in and isoprene- and monoterpene-rich atmosphere: constraints from aircraft
638 (SEAC⁴RS) and ground-based (SOAS) observations in the Southeast US, in preparation,
639 2016.

640 Fountoukis, C., and Nenes, A.: ISORROPIA II: A computationally efficient thermodynamic
641 equilibrium model for K⁺-Ca²⁺-Mg²⁺-NH₄⁺-Na⁺-SO₄²⁻-NO₃⁻-Cl⁻-H₂O aerosols, *Atmos.*
642 *Chem. Phys.*, 7, 4639-4659, doi:10.5194/acp-7-4639-2007, 2007.

643 Fu, T.-M., Jacob, D. J., Wittrock, F., Burrows, J. P., Vrekoussis, M., and Henze, D. K.: Global
644 budgets of atmospheric glyoxal and methylglyoxal, and implications for formation of
645 secondary organic aerosols, *J. Geophys. Res.*, 113, D15303, doi:10.1029/2007jd009505,
646 2008.

647 Fu, T.-M., Jacob, D. J., and Heald, C. L.: Aqueous-phase reactive uptake of dicarbonyls as a
648 source of organic aerosol over eastern North America, *Atmos. Environ.*, 43, 1814-1822,
649 doi:10.1016/j.atmosenv.2008.12.029, 2009.

650 Gaston, C. J., Riedel, T. P., Zhang, Z., Gold, A., Surratt, J. D., and Thornton, J. A.: Reactive
651 uptake of an isoprene-derived epoxydiol to submicron aerosol particles, *Environ. Sci.*
652 *Technol.*, 48, 11178-11186, doi:10.1021/es5034266, 2014.

653 González Abad, G. G., Liu, X., Chance, K., Wang, H., Kurosu, T. P., and Suleiman, R.: Updated
654 Smithsonian Astrophysical Observatory Ozone Monitoring Instrument (SAO OMI)
655 formaldehyde retrieval, *Atmos. Meas. Tech.*, 8, 19-32, doi:10.5194/amt-8-19-2015, 2015.

656 Guenther, A., Karl, T., Harley, P., Wiedinmyer, C., Palmer, P. I., and Geron, C.: Estimates of
657 global terrestrial isoprene emissions using MEGAN (Model of Emissions of Gases and
658 Aerosols from Nature), *Atmos. Chem. Phys.*, 6, 3181-3210, doi:10.5194/acp-6-3181-2006,
659 2006.

660 Guenther, A. B., Jiang, X., Heald, C. L., Sakulyanontvittaya, T., Duhl, T., Emmons, L. K., and
661 Wang, X.: The Model of Emissions of Gases and Aerosols from Nature version 2.1
662 (MEGAN2.1): An extended and updated framework for modeling biogenic emissions,
663 *Geosci. Model Dev.*, 5, 1471-1492, doi:10.5194/gmd-5-1471-2012, 2012.

664 Guo, H., Xu, L., Bougiatioti, A., Cerully, K. M., Capps, S. L., Hite Jr., J. R., Carlton, A. G., Lee,
665 S.-H., Bergin, M. H., Ng, N. L., Nenes, A., and Weber, R. J.: Fine-particle water and pH in
666 the southeastern United States, *Atmos. Chem. Phys.*, 15, 5211-5228, doi:10.5194/acp-15-
667 5211-2015, 2015.

668 Hallquist, M., Wenger, J. C., Baltensperger, U., Rudich, Y., Simpson, D., Claeys, M., Dommen,
669 J., Donahue, N. M., George, C., Goldstein, A. H., Hamilton, J. F., Herrmann, H.,
670 Hoffmann, T., Iinuma, Y., Jang, M., Jenkin, M. E., Jimenez, J. L., Kiendler-Scharr, A.,
671 Maenhaut, W., McFiggans, G., Mentel, Th. F., Monod, A., Prévôt, A. S. H., Seinfeld, J. H.,
672 Surratt, J. D., Szmigielski, R., and Wildt, J.: The formation, properties and impact of
673 secondary organic aerosol: Current and emerging issues, *Atmos. Chem. Phys.*, 9, 5155-
674 5236, doi:10.5194/acp-9-5155-2009, 2009.

675 Hess, M., Koepke, P., and Schult, I.: Optical properties of aerosols and clouds: The software
676 package OPAC, *B. Am. Meteorol. Soc.*, 79, 831-844, 1998.

677 Hodzic, A., and Jimenez, J. L.: Modeling anthropogenically controlled secondary organic
678 aerosols in a megacity: A simplified framework for global and climate models, *Geosci.*
679 *Model. Dev.*, 4, 901-917, doi:10.5194/gmd-4-901-2011, 2011.

680 Hu, K. S., Darer, A. I., and Elrod, M. J.: Thermodynamics and kinetics of the hydrolysis of
681 atmospherically relevant organonitrates and organosulfates, *Atmos. Chem. Phys.*, 11, 8307-
682 8320, doi:10.5194/acp-11-8307-2011, 2011.

683 Hu, W. W., Campuzano-Jost, P., Palm, B. B., Day, D. A., Ortega, A. M., Hayes, P. L.,
684 Krechmer, J. E., Chen, Q., Kuwata, M., Liu, Y. J., de Sá, S. S., Martin, S. T., Hu, M.,
685 Budisulistiorini, S. H., Riva, M., Surratt, J. D., St. Clair, J. M., Isaacman-Van Wertz, G.,
686 Yee, L. D., Goldstein, A. H., Carbone, S., Artaxo, P., de Gouw, J. A., Koss, A., Wisthaler,
687 A., Mikoviny, T., Karl, T., Kaser, L., Jud, W., Hansel, A., Docherty, K. S., Robinson, N. H.,
688 Coe, H., Allan, J. D., Canagaratna, M. R., Paulot, F., and Jimenez, J. L.: Characterization
689 of a real-time tracer for isoprene epoxydiols-derived secondary organic aerosol (IEPOX-
690 SOA) from aerosol mass spectrometer measurements, *Atmos. Chem. Phys.*, 15, 11807-
691 11833, doi:10.5194/acp-15-11807-2015, 2015.

- 692 Jacob, D. J.: Heterogeneous chemistry and tropospheric ozone, *Atmos. Environ.*, 34, 2131-2159,
693 doi:10.1016/s1352-2310(99)00462-8, 2000.
- 694 Jacobs, M. I., Darer, A. I., and Elrod, M. J.: Rate constants and products of the OH reaction with
695 isoprene-derived epoxides, *Environ. Sci. Technol.*, 47, 12868-12876,
696 doi:10.1021/es403340g, 2013.
- 697 Jacobs, M. I., Burke, W. J., and Elrod, M. J.: Kinetics of the reactions of isoprene-derived
698 hydroxynitrates: Gas phase epoxide formation and solution phase hydrolysis, *Atmos.*
699 *Chem. Phys.*, 14, 8933-8946, doi:10.5194/acp-14-8933-2014, 2014.
- 700 Kim, P. S., Jacob, D. J., Fisher, J. A., Travis, K., Yu, K., Zhu, L., Yantosca, R. M., Sulprizio, M.
701 P., Jimenez, J. L., Campuzano-Jost, P., Froyd, K. D., Liao, J., Hair, J. W., Fenn, M. A.,
702 Butler, C. F., Wagner, N. L., Gordon, T. D., Welti, A., Wennberg, P. O., Crounse, J. D., St.
703 Clair, J. M., Teng, A. P., Millet, D. B., Schwarz, J. P., Markovic M. Z., and Perring, A. E.:
704 Sources, seasonality, and trends of southeast US aerosol: an integrated analysis of surface,
705 aircraft, and satellite observations with the GEOS-Chem chemical transport model, *Atmos.*
706 *Chem. Phys.*, 15, 10411-10433, doi:10.5194/acpd-15-10411-2015, 2015.
- 707 King, S. M., Rosenoern, T., Shilling, J. E., Chen, Q., Wang, Z., Biskos, G., McKinney, K. A.,
708 Pöschl, U., and Martin, S. T.: Cloud droplet activation of mixed organic-sulfate particles
709 produced by the photooxidation of isoprene, *Atmos. Chem. Phys.*, 10, 3953-3964,
710 doi:10.5194/acp-10-3953-2010, 2010.
- 711 Kleindienst, T. E., Edney, E. O., Lewandowski, M., Offenberg, J. H., and Jaoui, M.: Secondary
712 organic carbon and aerosol yields from the irradiations of isoprene and α -pinene in the
713 presence of NO_x and SO₂, *Environ. Sci. Technol.*, 40, 3807-3812, doi:10.1021/es052446r,
714 2006.
- 715 Kleindienst, T. E., Lewandowski, M., Offenberg, J. H., Jaoui, M., and Edney, E. O.: Ozone-
716 isoprene reaction: Re-examination of the formation of secondary organic aerosol, *Geophys.*
717 *Res. Lett.*, 34, L01805, doi:10.1029/2006gl027485, 2007.
- 718 Kleindienst, T. E., Lewandowski, M., Offenberg, J. H., Jaoui, M., and Edney, E. O.: The
719 formation of secondary organic aerosol from the isoprene + OH reaction in the absence of
720 NO_x, *Atmos. Chem. Phys.*, 9, 6541-6558, doi:10.5194/acp-9-6541-2009, 2009.
- 721 Knote, C., Hodzic, A., Jimenez, J. L., Volkamer, R., Orlando, J. J., Baidar, S., Brioude, J., Fast,
722 J., Gentner, D. R., Goldstein, A. H., Hayes, P. L., Knighton, W. B., Oetjen, H., Setyan, A.,
723 Stark, H., Thalman, R., Tyndall, G., Washenfelder, R., Waxman, E., and Zhang, Q.:
724 Simulation of semi-explicit mechanisms of SOA formation from glyoxal in aerosol in a 3-
725 D model, *Atmos. Chem. Phys.*, 14, 6213-6239, doi:10.5194/acp-14-6213-2014, 2014.
- 726 Koepke, P., Hess, M., Schult, I., and Shettle, E. P.: Global aerosol data set, report, Max-Planck
727 Inst. für Meteorol., Hamburg, Germany, 1997.
- 728 Krechmer, J. E., Coggon, M. M., Massoli, P., Nguyen, T. B., Crounse, J. D., Hu, W., Day, D. A.,
729 Tyndall, G. S., Henze, D. K., Rivera-Rios, J. C., Nowak, J. B., Kimmel, J. R., Mauldin, III,
730 R. L., Stark, H., Jayne, J. T., Sipilä, M., Junninen, H., St. Clair, J. M., Zhang, X., Feiner, P.
731 A., Zhang, L., Miller, D. O., Brune, W. H., Keutsch, F. N., Wennberg, P. O., Seinfeld, J.
732 H., Worsnop, D. R., Jimenez, J. L., and Canagaratna, M. R.: Formation of low volatility
733 organic compounds and secondary organic aerosol from isoprene hydroxyhydroperoxide

734 low-NO oxidation, *Environ. Sci. Technol.*, 49, 10330-10339, doi:10.1021/acs.est.5b02031,
735 2015.

736 Kroll, J. H., Ng, N. L., Murphy, S. M., Flagan, R. C., and Seinfeld, J. H.: Secondary organic
737 aerosol formation from isoprene photooxidation under high-NO_x conditions, *Geophys. Res.*
738 *Lett.*, 32, L18808, doi:10.1029/2005gl023637, 2005.

739 Kroll, J. H., Ng, N. L., Murphy, S. M., Flagan, R. C., and Seinfeld, J. H.: Secondary organic
740 aerosol formation from isoprene photooxidation, *Environ. Sci. Technol.*, 40, 1869-1877,
741 doi:10.1021/es0524301, 2006.

742 Lee, L., Teng, A. P., Wennberg, P. O., Crouse, J. D., and Cohen, R. C.: On rates and
743 mechanisms of OH and O₃ reactions with isoprene-derived hydroxy nitrates, *J. Phys.*
744 *Chem. A*, 118, 1622-1637, doi:10.1021/jp4107603, 2014.

745 Lewandowski, M., Jaoui, M., Offenberg, J. H., Krug, J. D., and Kleindienst, T. E.: Atmospheric
746 oxidation of isoprene and 1,3-butadiene: Influence of aerosol acidity and relative humidity
747 on secondary organic aerosol, *Atmos. Chem. Phys.*, 15, 3773-3783, doi:10.5194/acp-15-
748 3773-2015, 2015.

749 Liao, J., Froyd, K. D., Murphy, D. M., Keutsch, F. N., Yu, G., Wennberg, P. O., St Clair, J. M.,
750 Crouse, J. D., Wisthaler, A., Mikoviny, T., Jimenez, J. L., Campuzano-Jost, P., Day, D.
751 A., Hu, W., Ryerson, T. B., Pollack, I. B., Peischl, J., Anderson, B. E., Ziemba, L. D.,
752 Blake, D. R., Meinardi, S., and Diskin, G.: Airborne measurements of organosulfates over
753 the continental U.S., *J. Geophys. Res.*, 120, 2990-3005, doi:10.1002/2014jd022378, 2015.

754 Liggió, J., Li, S.-M., and McLaren, R.: Reactive uptake of glyoxal by particulate matter, *J.*
755 *Geophys. Res.*, 110, D10304, doi:10.1029/2004jd005113, 2005.

756 Lin, Y.-H., Zhang, H., Pye, H. O. T., Zhang, Z. F., Marth, W. J., Park, S., Arashiro, M., Cui, T.,
757 Budisulistiorini, S. H., Sexton, K. G., Vizuete, W., Xie, Y., Luecken, D. J., Piletic, I. R.,
758 Edney, E. O., Bartolotti, L. J., Gold, A., and Surratt, J. D.: Epoxide as a precursor to
759 secondary organic aerosol formation from isoprene photooxidation in the presence of
760 nitrogen oxides, *P. Natl. Acad. Sci. USA*, 110, 6718-6723, doi:10.1073/pnas.1221150110,
761 2013.

762 Liu, Y. J., Herdinger-Blatt, I., McKinney, K. A., and Martin, S. T.: Production of methyl vinyl
763 ketone and methacrolein via the hydroperoxyl pathway of isoprene oxidation, *Atmos.*
764 *Chem. Phys.*, 13, 5715-5730, doi:10.5194/acp-13-5715-2013, 2013.

765 Lin, G., S. Sillman, J. E. Penner, and A. Ito, Global modeling of SOA: the use of different
766 mechanisms for aqueous-phase formation, *Atmos. Chem. Phys.*, 14, 5451-5475,
767 doi:10.5194/acp-14-5451-2014, 2014.

768 Liu, J., L. W. Horowitz, S. Fan, A. G. Carlton, and H. Levy II, Global in-cloud production of
769 secondary organic aerosols: implementation of a detailed chemical mechanism in the
770 GFDL atmospheric model AM3, *J. Geophys. Res.*, D117, D15303,
771 doi:10.1029/2012JD017838, 2012.

772 Mao, J., Paulot, F., Jacob, D. J., Cohen, R. C., Crouse, J. D., Wennberg, P. O., Keller, C. A.,
773 Hudman, R. C., Barkley, M. P., and Horowitz, L. W.: Ozone and organic nitrates over the
774 eastern United States: Sensitivity to isoprene chemistry, *J. Geophys. Res.*, 118, 11256-
775 11268, doi:10.1002/jgrd.50817, 2013.

776 Martin, R. V., Jacob, D. J., Yantosca, R. M., Chin, M., and Ginoux, P.: Global and regional
777 decreases in tropospheric oxidants from photochemical effects of aerosols, *J. Geophys.*
778 *Res.*, 108, 4097, doi:10.1029/2002jd002622, 2003.

779 McNeill, V. F., Woo, J. L., Kim, D. D., Schwier, A. N., Wannell, N. J., Sumner, A. J., and
780 Barakat, J. M.: Aqueous-phase secondary organic aerosol and organosulfate formation in
781 atmospheric aerosols: A modeling study, *Environ. Sci. Technol.*, 46, 8075-8081,
782 doi:10.1021/es3002986, 2012.

783 McNeill, V. F., Sareen, N., and Schwier, A. N.: Surface-active organics in atmospheric aerosols,
784 *Top. Curr. Chem.*, 339, 201-259, doi:10.1007/128_2012_404, 2014.

785 Millet, D. B., Jacob, D. J., Turquety, S., Hudman, R. C., Wu, S., Fried, A., Walega, J., Heikes, B.
786 G., Blake, D. R., Singh, H. B., Anderson, B. E., and Clarke, A. D.: Formaldehyde
787 distribution over North America: Implications for satellite retrievals of formaldehyde
788 columns and isoprene emission, *J. Geophys. Res.*, 111, D24S02,
789 doi:10.1029/2005jd006853, 2006.

790 Myriokefalitakis, S., Tsigaridas, K., Mihalopoulos, N., Sciare, J., Nenes, A., Kawamura, K.,
791 Segers, A., and Kanakidou, M.: In-cloud oxalate formation in the global troposphere: a 3-D
792 modeling study, *Atmos. Chem. Phys.*, 11, 5761-5782, doi:10.5194/acp-11-5761-2011,
793 2011.

794 Ng, N. L., Kwan, A. J., Surratt, J. D., Chan, A. W. H., Chhabra, P. S., Sorooshian, A., Pye, H. O.
795 T., Crouse, J. D., Wennberg, P. O., Flagan, R. C., and Seinfeld, J. H.: Secondary organic
796 aerosol (SOA) formation from reaction of isoprene with nitrate radicals (NO₃), *Atmos.*
797 *Chem. Phys.*, 8, 4117-4140, doi:10.5194/acp-8-4117-2008, 2008.

798 Nguyen, T. B., Coggon, M. M., Bates, K. H., Zhang, X., Schwantes, R. H., Schilling, K. A.,
799 Loza, C. L., Flagan, R. C., Wennberg, P. O., and Seinfeld, J. H.: Organic aerosol formation
800 from the reactive uptake of isoprene epoxydiols (IEPOX) onto non-acidified inorganic
801 seeds, *Atmos. Chem. Phys.*, 14, 3497-3510, doi:10.5194/acp-14-3497-2014, 2014.

802 Nguyen, T. B., Crouse, J. D., Teng, A. P., St. Clair, J. M., Paulot, F., Wolfe, G. M., and
803 Wennberg, P. O.: Rapid deposition of oxidized biogenic compounds to a temperate forest,
804 *P. Natl. Acad. Sci. USA*, 112, E392-E401, doi:10.1073/pnas.1418702112, 2015a.

805 Nguyen, T. B., Bates, K. H., Crouse, J. D., Schwantes, R. H., Zhang, X., Kjaergaard, H. G.,
806 Surratt, J. D., Lin, P., Laskin, A., Seinfeld, J. H., and Wennberg, P. O.: Mechanism of the
807 hydroxyl radical oxidation of methacryloyl peroxyxynitrate (MPAN) and its pathway toward
808 secondary organic aerosol formation in the atmosphere, *Phys Chem Chem Phys*, 17, 17914-
809 17926, doi:10.1039/c5cp02001h, 2015b.

810 Nozière, B., Dziedzic, P., and Córdoba, A.: Products and kinetics of the liquid-phase reaction of
811 glyoxal catalyzed by ammonium ions (NH₄⁺), *J. Phys. Chem. A*, 113, 231-237,
812 doi:10.1021/jp8078293, 2009.

813 Odum, J. R., Hoffmann, T., Bowman, F., Collins, D., Flagan, R. C., and Seinfeld, J. H.:
814 Gas/particle partitioning and secondary organic aerosol yields, *Environ. Sci. Technol.*, 30,
815 2580-2585, doi:10.1021/es950943+, 1996.

- 816 Palmer, P. I., Jacob, D. J., Fiore, A. M., Martin, R. V., Chance, K., and Kurosu, T. P.: Mapping
817 isoprene emissions over North America using formaldehyde column observations from
818 space, *J. Geophys. Res.*, 108, 4180, doi:10.1029/2002jd002153, 2003.
- 819 Palmer, P. I., Abbot, D. S., Fu, T.-M., Jacob, D. J., Chance, K., Kurosu, T. P., Guenther, A.,
820 Wiedinmyer, C., Stanton, J. C., Pilling, M. J., Pressley, S. N., Lamb, B., and Sumner, A. L.:
821 Quantifying the seasonal and interannual variability of North American isoprene emissions
822 using satellite observations of the formaldehyde column, *J. Geophys. Res.*, 111, D12315,
823 doi:10.1029/2005jd006689, 2006.
- 824 Paulot, F., Crouse, J. D., Kjaergaard, H. G., Kroll, J. H., Seinfeld, J. H., and Wennberg, P. O.:
825 Isoprene photooxidation: New insights into the production of acids and organic nitrates,
826 *Atmos. Chem. Phys.*, 9, 1479-1501, doi:10.5194/acp-9-1479-2009, 2009a.
- 827 Paulot, F., Crouse, J. D., Kjaergaard, H. G., Kürten, A., St Clair, J. M., Seinfeld, J. H., and
828 Wennberg, P. O.: Unexpected epoxide formation in the gas-phase photooxidation of
829 isoprene, *Science*, 325, 730-733, doi:10.1126/science.1172910, 2009b.
- 830 Peeters, J., Nguyen, T. L., and Vereecken, L.: HO_x radical regeneration in the oxidation of
831 isoprene, *Phys. Chem. Chem. Phys.*, 11, 5935-5939, doi:10.1039/b908511d, 2009.
- 832 Peeters, J., and Müller, J.-F.: HO_x radical regeneration in isoprene oxidation via peroxy radical
833 isomerisations. II: Experimental evidence and global impact, *Phys. Chem. Chem. Phys.*, 12,
834 14227-14235, doi:10.1039/c0cp00811g, 2010.
- 835 Piletic, I. R., Edney, E. O., and Bartolotti, L. J.: A computational study of acid catalyzed aerosol
836 reactions of atmospherically relevant epoxides, *Phys. Chem. Chem. Phys.*, 15, 18065-
837 18076, doi:10.1039/c3cp52851k, 2013.
- 838 Pye, H. O. T., Chan, A. W. H., Barkley, M. P., and Seinfeld, J. H.: Global modeling of organic
839 aerosol: The importance of reactive nitrogen (NO_x and NO₃), *Atmos. Chem. Phys.*, 10,
840 11261-11276, doi:10.5194/acp-10-11261-2010, 2010.
- 841 Pye, H. O. T., Pinder, R. W., Piletic, I. R., Xie, Y., Capps, S. L., Lin, Y.-H., Surratt, J. D., Zhang,
842 Z., Gold, A., Luecken, D. J., Hutzell, W. T., Jaoui, M., Offenberg, J. H., Kleindienst, T. E.,
843 Lewandowski, M., and Edney, E. O.: Epoxide pathways improve model predictions of
844 isoprene markers and reveal key role of acidity in aerosol formation, *Environ. Sci.*
845 *Technol.*, 47, 11056-11064, doi:10.1021/es402106h, 2013.
- 846 Riedel, T. P., Lin, Y.-H., Budisulistiorini, S. H., Gaston, C. J., Thornton, J. A., Zhang, Z. F.,
847 Vizuete, W., Gold, A., and Surratt, J. D.: Heterogeneous reactions of isoprene-derived
848 epoxides: Reaction probabilities and molar secondary organic aerosol yield estimates,
849 *Environ. Sci. Technol. Lett.*, 2, 38-42, doi:10.1021/ez500406f, 2015.
- 850 Rollins, A. W., Kiendler-Scharr, A., Fry, J. L., Brauers, T., Brown, S. S., Dorn, H.-P., Dubé, W.
851 P., Fuchs, H., Mensah, A., Mentel, T. F., Rohrer, F., Tillmann, R., Wegener, R.,
852 Wooldridge, P. J., and Cohen, R. C.: Isoprene oxidation by nitrate radical: Alkyl nitrate and
853 secondary organic aerosol yields, *Atmos. Chem. Phys.*, 9, 6685-6703, doi:10.5194/acp-9-
854 6685-2009, 2009.
- 855 SEAC⁴RS Archive, doi:10.5067/Aircraft/SEAC4RS/Aerosol-TraceGas-Cloud.

- 856 Sato, K., Nakao, S., Clark, C. H., Qi, L., and Cocker III, D. R.: Secondary organic aerosol
857 formation from the photooxidation of isoprene, 1,3-butadiene, and 2,3-dimethyl-1,3-
858 butadiene under high NO_x conditions, *Atmos. Chem. Phys.*, 11, 7301-7317,
859 doi:10.5194/acp-11-7301-2011, 2011.
- 860 Saxena, P., and Hildemann, L. M.: Water-soluble organics in atmospheric particles: A critical
861 review of the literature and application of thermodynamics to identify candidate
862 compounds, *J. Atmos. Chem.*, 24, 57-109, doi:10.1007/bf00053823, 1996.
- 863 Schwartz, S.E.: Mass-transport considerations pertinent to aqueous-phase reactions of gases in
864 liquid-water clouds. In: Jaechske, W. (Ed.), *Chemistry of Multiphase Atmospheric*
865 *Systems*, Springer, Heidelberg, pp. 415-471, 1986.
- 866 Scott, C. E., Rap, A., Spracklen, D. V., Forster, P. M., Carslaw, K. S., Mann, G. W., Pringle, K.
867 J., Kivekäs, N., Kulmala, M., Lihavainen, H., and Tunved, P.: The direct and indirect
868 radiative effects of biogenic secondary organic aerosol, *Atmos. Chem. Phys.*, 14, 447-470,
869 doi:10.5194/acp-14-447-2014, 2014.
- 870 Song, M., Liu, P. F., Hanna, S. J., Li, Y. J., Martin, S. T., and Bertram, A. K.: Relative humidity-
871 dependent viscosities of isoprene-derived secondary organic material and atmospheric
872 implications for isoprene-dominant forests, *Atmos. Chem. Phys.*, 15, 5145-5159,
873 doi:10.5194/acp-15-5145-2015, 2015.
- 874 Stavrou, T., Peeters, J., and Müller, J.-F.: Improved global modelling of HO_x recycling in
875 isoprene oxidation: Evaluation against the GABRIEL and INTEX-A aircraft campaign
876 measurements, *Atmos. Chem. Phys.*, 10, 9863-9878, doi:10.5194/acp-10-9863-2010, 2010.
- 877 St. Clair, J. M., Rivera-Rios, J. C., Crouse, J. D., Knap, H. C., Bates, K. H., Teng, A. P.,
878 Jørgensen, S., Kjaergaard, H. G., Keutsch, F. N., Wennberg, P. O.: Kinetics and products
879 of the reaction of the first-generation isoprene hydroperoxide (ISOPPOOH) with OH, *J.*
880 *Phys. Chem. A*, doi:10.1021/acs.jpca.5b06532, 2016.
- 881 Sumner, A. J., Woo, J. L., and McNeill, V. F.: Model Analysis of secondary organic aerosol
882 formation by glyoxal in laboratory studies: The case for photoenhanced chemistry,
883 *Environ. Sci. Technol.*, 48, 11919-11925, doi:10.1021/es502020j, 2014.
- 884 Surratt, J. D., Murphy, S. M., Kroll, J. H., Ng, N. L., Hildebrandt, L., Sorooshian, A.,
885 Szmigielski, R., Vermeylen, R., Maenhaut, W., Claeys, M., Flagan, R. C., and Seinfeld, J.
886 H.: Chemical composition of secondary organic aerosol formed from the photooxidation of
887 isoprene, *J. Phys. Chem. A*, 110, 9665-9690, doi:10.1021/jp061734m, 2006.
- 888 Surratt, J. D., Lewandowski, M., Offenber, J. H., Jaoui, M., Kleindienst, T. E., Edney, E. O.,
889 and Seinfeld, J. H.: Effect of acidity on secondary organic aerosol formation from isoprene,
890 *Environ. Sci. Technol.*, 41, 5363-5369, doi:10.1021/es0704176, 2007a.
- 891 Surratt, J. D., Kroll, J. H., Kleindienst, T. E., Edney, E. O., Claeys, M., Sorooshian, A., Ng, N.
892 L., Offenber, J. H., Lewandowski, M., Jaoui, M., Flagan, R. C., and Seinfeld, J. H.:
893 Evidence for organosulfates in secondary organic aerosol, *Environ. Sci. Technol.*, 41, 517-
894 527, doi:10.1021/es062081q, 2007b.
- 895 Surratt, J. D., Chan, A. W. H., Eddingsaas, N. C., Chan, M., Loza, C. L., Kwan, A. J., Hersey, S.
896 P., Flagan, R. C., Wennberg, P. O., and Seinfeld, J. H.: Reactive intermediates revealed in

- 897 secondary organic aerosol formation from isoprene, *P. Natl. Acad. Sci. USA*, 107, 6640-
898 6645, doi:10.1073/pnas.0911114107, 2010.
- 899 Tan, Y., Perri, M. J., Seitzinger, S. P., and Turpin, B. J.: Effects of precursor concentration and
900 acidic sulfate in aqueous glyoxal-OH radical oxidation and implications for secondary
901 organic aerosol, *Environ. Sci. Technol.*, 43, 8105-8112, doi:10.1021/es901742f, 2009.
- 902 Tan, Y., Carlton, A. G., Seitzinger, S. P., and Turpin, B. J.: SOA from methylglyoxal in clouds
903 and wet aerosols: Measurement and prediction of key products, *Atmos. Environ.*, 44, 5218-
904 5226, doi:10.1016/j.atmosenv.2010.08.045, 2010.
- 905 Toon, O. B. and the SEAC⁴RS science team: Planning, implementation, and scientific goals of
906 the Studies of Emissions and Atmospheric Composition, Clouds, and Climate Coupling by
907 Regional Surveys (SEAC⁴RS) field mission, submitted to *J. Geophys. Res.*, 2016.
- 908 Travis, K. R., Jacob, D. J., Fisher, J. A., Kim, P. S., Marais, E. A., Zhu, L., Miller, C. C.,
909 Wennberg, P. O., Crounse, J., Hanisco, T. A., Ryerson, T., Yu, K., Wolfe, G. M.,
910 Thompson, A., Mao, J., Paulot, F., Yantosca, R. M., Sulprizio, M., and Neuman, A.: NO_x
911 emissions, isoprene oxidation pathways, and implications for surface ozone in the
912 Southeast United States, in preparation, 2016.
- 913 Virtanen, A., Joutsensaari, J., Koop, T., Kannosto, J., Yli-Pirilä, P., Leskinen, J., Mäkelä, J. M.,
914 Holopainen, J. K., Pöschl, U., Kulmala, M., Worsnop, D. R., and Laaksonen, A.: An
915 amorphous solid state of biogenic secondary organic aerosol particles, *Nature*, 467, 824-
916 827, doi:10.1038/nature09455, 2010.
- 917 Volkamer, R., Martini, F. S., Molina, L. T., Salcedo, D., Jimenez, J. L., and Molina, M. J.: A
918 missing sink for gas-phase glyoxal in Mexico City: Formation of secondary organic
919 aerosol, *Geophys. Res. Lett.*, 34, L19807, doi:10.1029/2007gl030752, 2007.
- 920 Volkamer, R., Ziemann, P. J., and Molina, M. J.: Secondary organic aerosol formation from
921 acetylene (C₂H₂): Seed effect on SOA yields due to organic photochemistry in the aerosol
922 aqueous phase, *Atmos. Chem. Phys.*, 9, 1907-1928, doi:10.5194/acp-9-1907-2009, 2009.
- 923 Wagner, N. L., Brock, C. A., Angevine, W. M., Beyersdorf, A., Campuzano-Jost, P., Day, D., de
924 Gouw, J. A., Diskin, G. S., Gordon, T. D., Graus, M. G., Holloway, J. S., Huey, G.,
925 Jimenez, J. L., Lack, D. A., Liao, J., Liu, X., Markovic, M. Z., Middlebrook, A. M.,
926 Mikoviny, T., Peischl, J., Perring, A. E., Richardson, M. S., Ryerson, T. B., Schwarz, J. P.,
927 Warneke, C., Welti, A., Wisthaler, A., Ziemba, L. D., and Murphy, D. M.: In situ vertical
928 profiles of aerosol extinction, mass, and composition over the southeast United States
929 during SENEX and SEAC⁴RS: Observations of a modest aerosol enhancement aloft,
930 *Atmos. Chem. Phys.*, 15, 7085-7102, doi:10.5194/acp-15-7085-2015, 2015.
- 931 Wang, J., Hoffmann, A. A., Park, R. J., Jacob, D. J., and Martin, S. T.: Global distribution of
932 solid and aqueous sulfate aerosols: Effect of the hysteresis of particle phase transitions, *J.*
933 *Geophys. Res.*, 113, D11206, doi:10.1029/2007jd009367, 2008.
- 934 Waxman, E. M., Dzepina, K., Ervens, B., Lee-Taylor, J., Aumont, B., Jimenez, J. L., Madronich,
935 S., and Volkamer, R.: Secondary organic aerosol formation from semi- and intermediate-
936 volatility organic compounds and glyoxal: Relevance of O/C as a tracer for aqueous
937 multiphase chemistry, *Geophys. Res. Lett.*, 40, 978-982, doi:10.1002/grl.50203, 2013.

- 938 Xu, L., Kollman, M. S., Song, C., Shilling, J. E., and Ng, N. L.: Effects of NO_x on the volatility
939 of secondary organic aerosol from isoprene photooxidation, *Environ. Sci. Technol.*, 48,
940 2253-2262, doi:10.1021/es404842g, 2014.
- 941 Xu, L., Guo, H., Boyd, C. M., Klein, M., Bougiatioti, A., Cerully, K. M., Hite, J. R., Isaacman-
942 VanWertz, G., Kreisberg, N. M., Knote, C., Olson, K., Koss, A., Goldstein, A. H., Hering,
943 S. V., de Gouw, J., Baumann, K., Lee, S.-H., Nenes, A., Weber, R. J., and Ng, N. L.:
944 Effects of anthropogenic emissions on aerosol formation from isoprene and monoterpenes
945 in the southeastern United States, *P. Natl. Acad. Sci. USA*, 112, 37-42,
946 doi:10.1073/pnas.1417609112, 2015.
- 947 Yu, K., Jacob, D. J., Fisher, J., Kim, P. S., Marais, E. A., Miller, C. C., Travis, K., Zhu, L.,
948 Yantosca, R. M., Sulprizio, M., Cohen, R. C., Dibb, J. E., Fried, A., Mikoviny, T., Ryerson,
949 T. B., Wennberg, P. O., and Wisthaler, A.: Sensitivity to grid resolution in the ability of a
950 chemical transport model to simulate observed oxidant chemistry under high-isoprene
951 conditions, submitted to *Atmos. Chem. Phys.*, 2016.
- 952 Zhang, Q., Jimenez, J. L., Canagaratna, M. R., Allan, J. D., Coe, H., Ulbrich, I., Alfarra, M. R.,
953 Takami, A., Middlebrook, A. M., Sun, Y. L., Dzepina, K., Dunlea, E., Docherty, K.,
954 DeCarlo, P. F., Salcedo, D., Onasch, T., Jayne, J. T., Miyoshi, T., Shimonono, A.,
955 Hatakeyama, S., Takegawa, N., Kondo, Y., Schneider, J., Drewnick, F., Borrmann, S.,
956 Weimer, S., Demerjian, K., Williams, P., Bower, K., Bahreini, R., Cottrell, L., Griffin, R.
957 J., Rautiainen, J., Sun, J. Y., Zhang, Y. M., and Worsnop, D. R.: Ubiquity and dominance
958 of oxygenated species in organic aerosols in anthropogenically-influenced Northern
959 Hemisphere midlatitudes, *Geophys. Res. Lett.*, 34, L13801, doi:10.1029/2007gl029979,
960 2007.
- 961 Zhang, H., Surratt, J. D., Lin, Y. H., Bapat, J., and Kamens, R. M.: Effect of relative humidity on
962 SOA formation from isoprene/NO photooxidation: Enhancement of 2-methylglyceric acid
963 and its corresponding oligoesters under dry conditions, *Atmos. Chem. Phys.*, 11, 6411-
964 6424, doi:10.5194/acp-11-6411-2011, 2011.
- 965 Zhang, H., Parikh, H. M., Bapat, J., Lin, Y. H., Surratt, J. D., and Kamens, R. M.: Modelling of
966 secondary organic aerosol formation from isoprene photooxidation chamber studies using
967 different approaches, *Environ. Chem.*, 10, 194-209, doi:10.1071/en13029, 2013.
- 968 Zhu, L., Jacob, D., Mickley, L., Kim, P. S., Fisher, J., Travis, K., Yu, K., Yantosca, R. M.,
969 Sulprizio, M., Fried, A., Hanisco, T., Wolfe, G., Abad, G. G., Chance, K., De Smedt, I.,
970 and Yang, K.: Indirect validation of new OMI, GOME-2, and OMPS formaldehyde
971 (HCHO) retrievals using SEAC⁴RS data, in preparation, 2016.

972 **TABLES**973 **Table 1.** Constants for reactive uptake of isoprene SOA precursors ^a

Species ^b	H^* [M atm ⁻¹]	k_{H^+} [M ⁻¹ s ⁻¹]	k_{nuc} [M ⁻² s ⁻¹]	$k_{HSO_4^-}$ [M ⁻¹ s ⁻¹]	k_{aq} [s ⁻¹]
IEPOX	$3.3 \times 10^7, ^c$	$3.6 \times 10^{-2}, ^d$	$2.0 \times 10^{-4}, ^e$	$7.3 \times 10^{-4}, ^e$	Equation (2)
ISOPN _β ^f	$3.3 \times 10^5, ^g$	–	–	–	$1.6 \times 10^{-5}, ^h$
ISOPN _δ ^f	$3.3 \times 10^5, ^g$	–	–	–	$6.8 \times 10^{-3}, ^h$
DHDN	$3.3 \times 10^5, ^g$	–	–	–	$6.8 \times 10^{-3}, ^i$

974 ^a Effective Henry's law constants H^* and aqueous-phase rate constants used to calculate reactive uptake
 975 coefficients γ for isoprene SOA precursors IEPOX, ISOPN_β, ISOPN_δ, and DHDN following Eqs. (1) and
 976 (2). Calculation of γ for other isoprene SOA precursors in Fig. 2 is described in the text.

977 ^b See Fig. 2 for definition of acronyms.

978 ^c Nguyen et al. (2014).

979 ^d Cole-Filipiak et al. (2010).

980 ^e Eddingsaas et al. (2010).

981 ^f ISOPN species formed from the beta and delta isoprene oxidation channels (Paulot et al., 2009a) are
 982 treated separately in GEOS-Chem.

983 ^g By analogy with 4-nitrooxy-3-methyl-2-butanol (Rollins et al., 2009).

984 ^h Jacobs et al. (2014).

985 ⁱ Assumed same as for ISOPN_δ (Hu et al., 2011).

986 **Table 2.** Mean reactive uptake coefficients γ of isoprene SOA precursors ^a

Species ^b	γ	pH dependence ^c			
		pH > 3	2 < pH < 3	1 < pH < 2	0 < pH < 1
IEPOX	4.2×10^{-3}	8.6×10^{-7}	2.0×10^{-4}	1.1×10^{-3}	1.0×10^{-2}
MEPOX	1.3×10^{-4}	2.7×10^{-8}	6.4×10^{-6}	3.6×10^{-5}	3.2×10^{-4}
ISOPN _{β}	1.3×10^{-7}	–			
ISOPN _{δ}	5.2×10^{-5}	–			
DHDN	6.5×10^{-5}	–			
GLYX	$2.9 \times 10^{-3, d}$	–			
MGLY	4.0×10^{-7}	–			
C ₅ -LVOC	0.1	–			
NT-ISOPN	0.1	–			

987 ^a Mean values computed in GEOS-Chem for the Southeast US in summer as sampled along the boundary-
 988 layer (< 2 km) SEAC⁴RS aircraft tracks and applied to aqueous aerosol. The reactive uptake coefficient γ
 989 is defined as the probability that a gas molecule colliding with an aqueous aerosol particle will be taken
 990 up and react in the aqueous phase to form non-volatile products.

991 ^b See Fig. 2 for definition of acronyms.

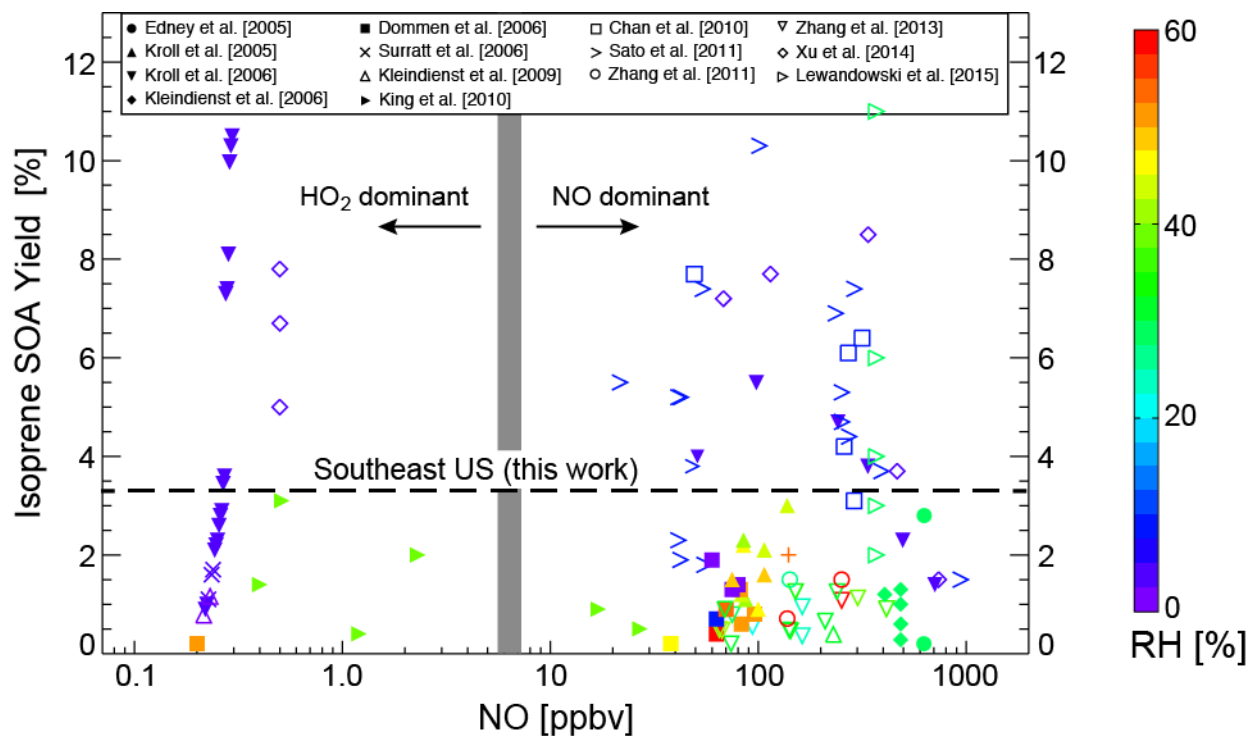
992 ^c γ for IEPOX and MEPOX are continuous functions of pH (Eq. (2)). Values shown here are averages for
 993 different pH ranges sampled along the SEAC⁴RS flight tracks. Aqueous aerosol pH is calculated locally
 994 in GEOS-Chem using the ISORROPIA thermodynamic model (Fountoukis and Nenes, 2007).

995 ^d Daytime value. Nighttime value is 5×10^{-6} .

996

997 **FIGURES**

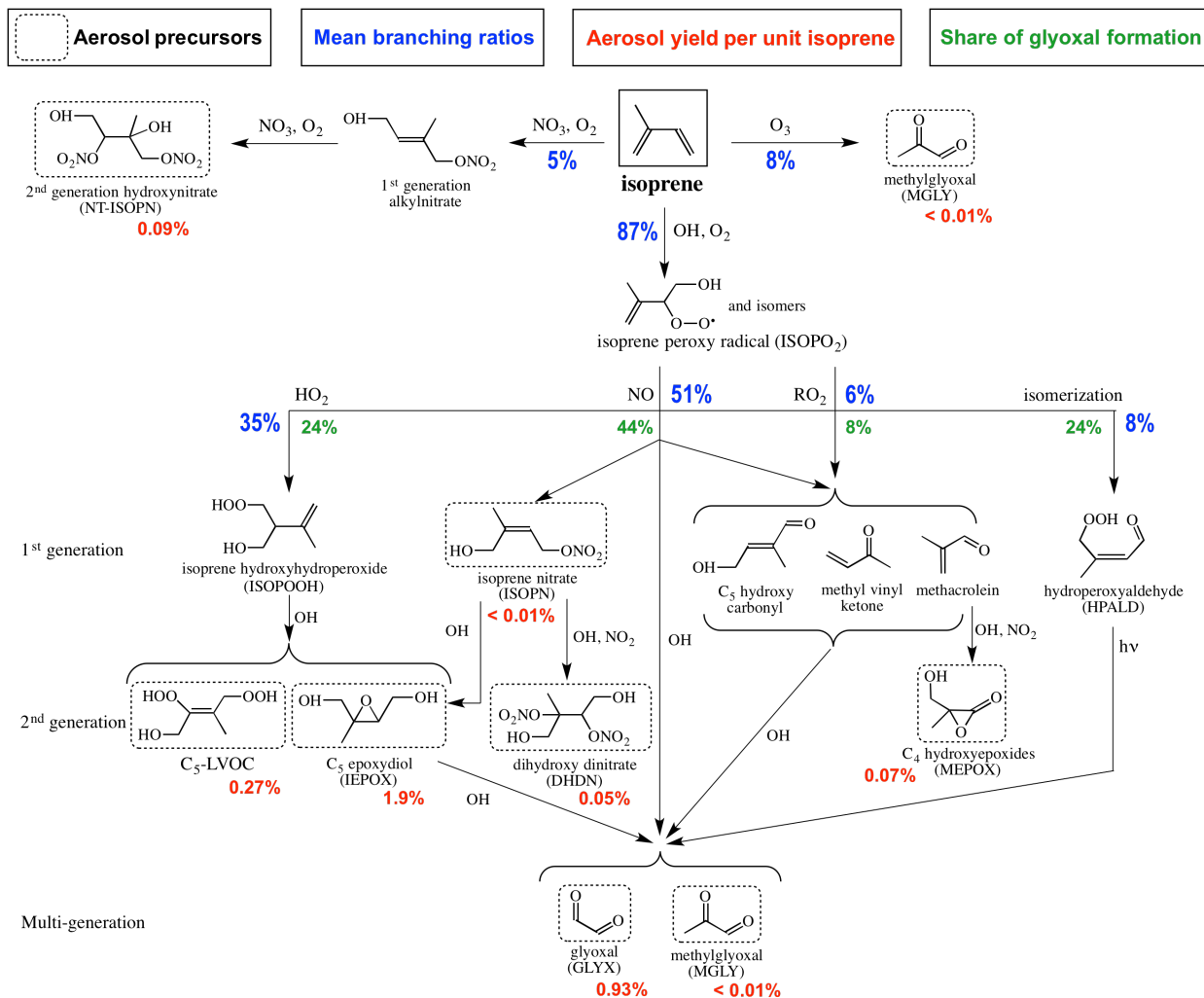
998



999

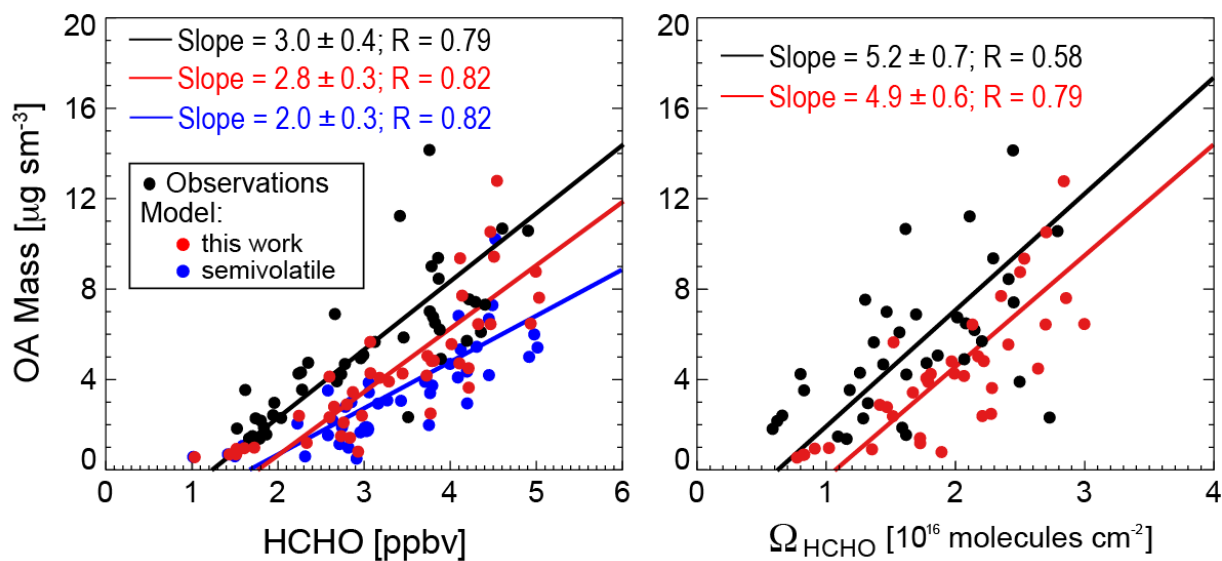
1000

1001 **Figure 1.** Yields of secondary organic aerosol (SOA) from isoprene oxidation as reported by
 1002 chamber studies in the literature and plotted as a function of the initial NO concentration and
 1003 relative humidity (RH). Yields are defined as the mass of SOA produced per unit mass of
 1004 isoprene oxidized. For studies with no detectable NO we plot the NO concentration as half the
 1005 reported instrument detection limit, and stagger points as needed for clarity. Data are colored by
 1006 relative humidity (RH). The thick grey line divides the low-NO_x and high-NO_x pathways as
 1007 determined by the fate of the ISOPO₂ radical (HO₂ dominant for the low-NO_x pathway, NO
 1008 dominant for the high-NO_x pathway). The transition between the two pathways occurs at a
 1009 higher NO concentration than in the atmosphere because HO₂ concentrations in the chambers are
 1010 usually much higher. Also shown as dashed line is the mean atmospheric yield of 3.3% for the
 1011 Southeast US determined in our study.



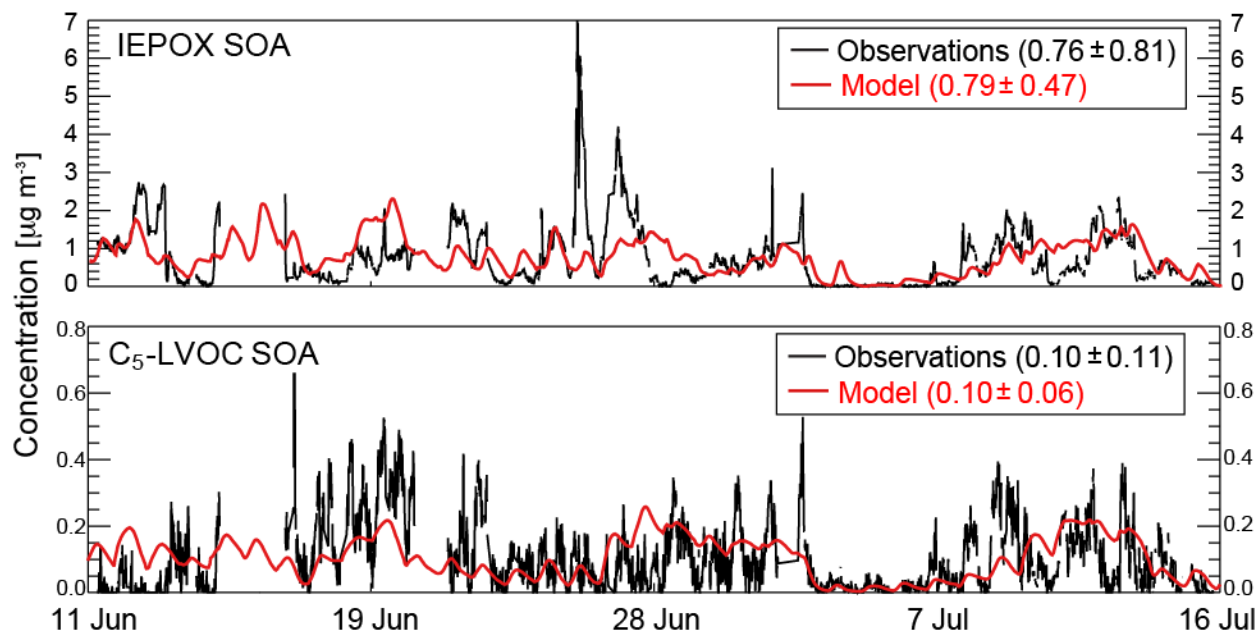
1012

1013 **Figure 2.** Gas-phase isoprene oxidation cascade in GEOS-Chem leading to secondary organic
 1014 aerosol (SOA) formation by irreversible aqueous-phase chemistry. Only selected species relevant
 1015 to SOA formation are shown. Immediate aerosol precursors are indicated by dashed boxes.
 1016 Branching ratios and SOA yields (aerosol mass produced per unit mass isoprene reacted) are
 1017 mean values from our GEOS-Chem simulation for the Southeast US boundary layer in summer.
 1018 The total SOA yield from isoprene oxidation is 3.3% and the values shown below the dashed
 1019 boxes indicate the contributions from the different immediate precursors adding up to 3.3%.
 1020 Contributions of high- and low-NO_x isoprene oxidation pathways to glyoxal are indicated.



1021

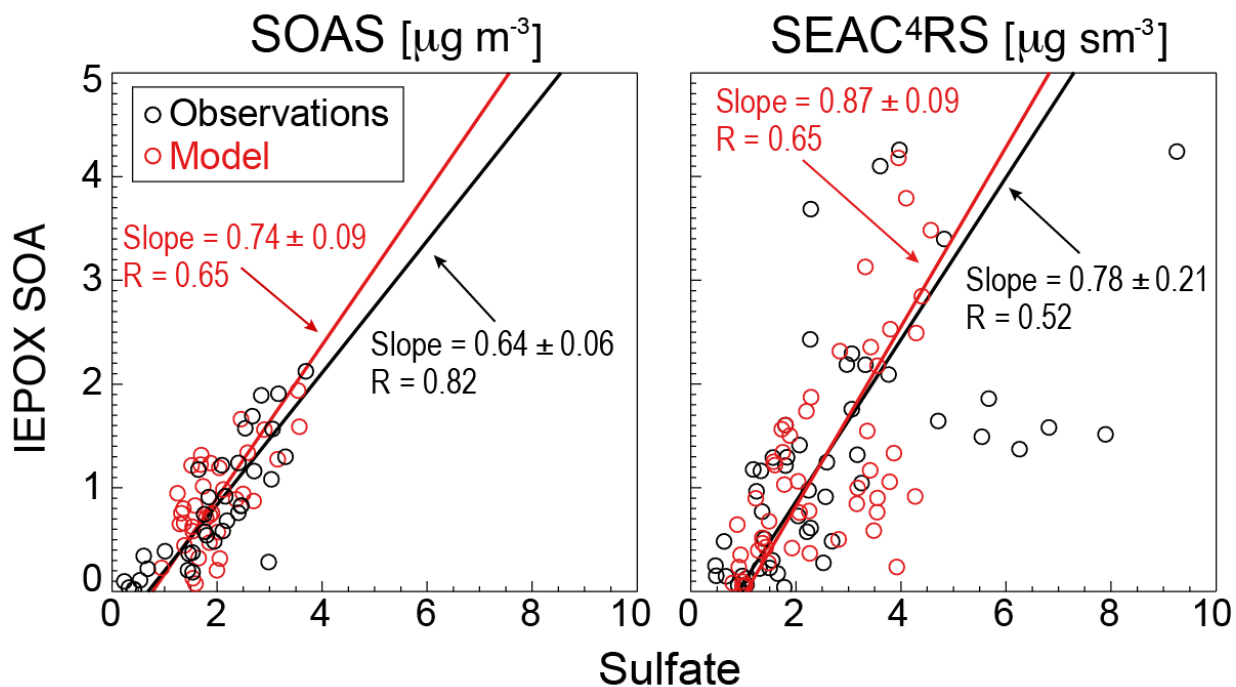
1022 **Figure 3.** Relationship of organic aerosol (OA) and formaldehyde (HCHO) concentrations over
 1023 the Southeast US in summer. The figure shows scatterplots of SEAC⁴RS aircraft observations of
 1024 OA concentrations in the boundary layer (< 2 km) vs. HCHO mixing ratios measured from the
 1025 aircraft (left), and column HCHO (Ω_{HCHO}) retrieved from OMI satellite observations (right).
 1026 Individual points are data from individual SEAC⁴RS flight days (August 8 - September 10),
 1027 averaged on the GEOS-Chem grid. OMI data are for SEAC⁴RS flight days and coincident with
 1028 the flight tracks. GEOS-Chem is sampled for the corresponding locations and times. Results
 1029 from our simulation with aqueous-phase isoprene SOA chemistry are shown in red, and results
 1030 from a simulation with the Pye et al. (2010) semivolatile reversible partitioning scheme are
 1031 shown in blue. Aerosol concentrations are per m^3 at standard conditions of temperature and
 1032 pressure (STP: 273 K; 1 atm), denoted sm^{-3} . Reduced major axis (RMA) regressions are also
 1033 shown with regression parameters and Pearson's correlation coefficients given inset. 1σ standard
 1034 deviations on the regression slopes are obtained with jackknife resampling.



1035

1036

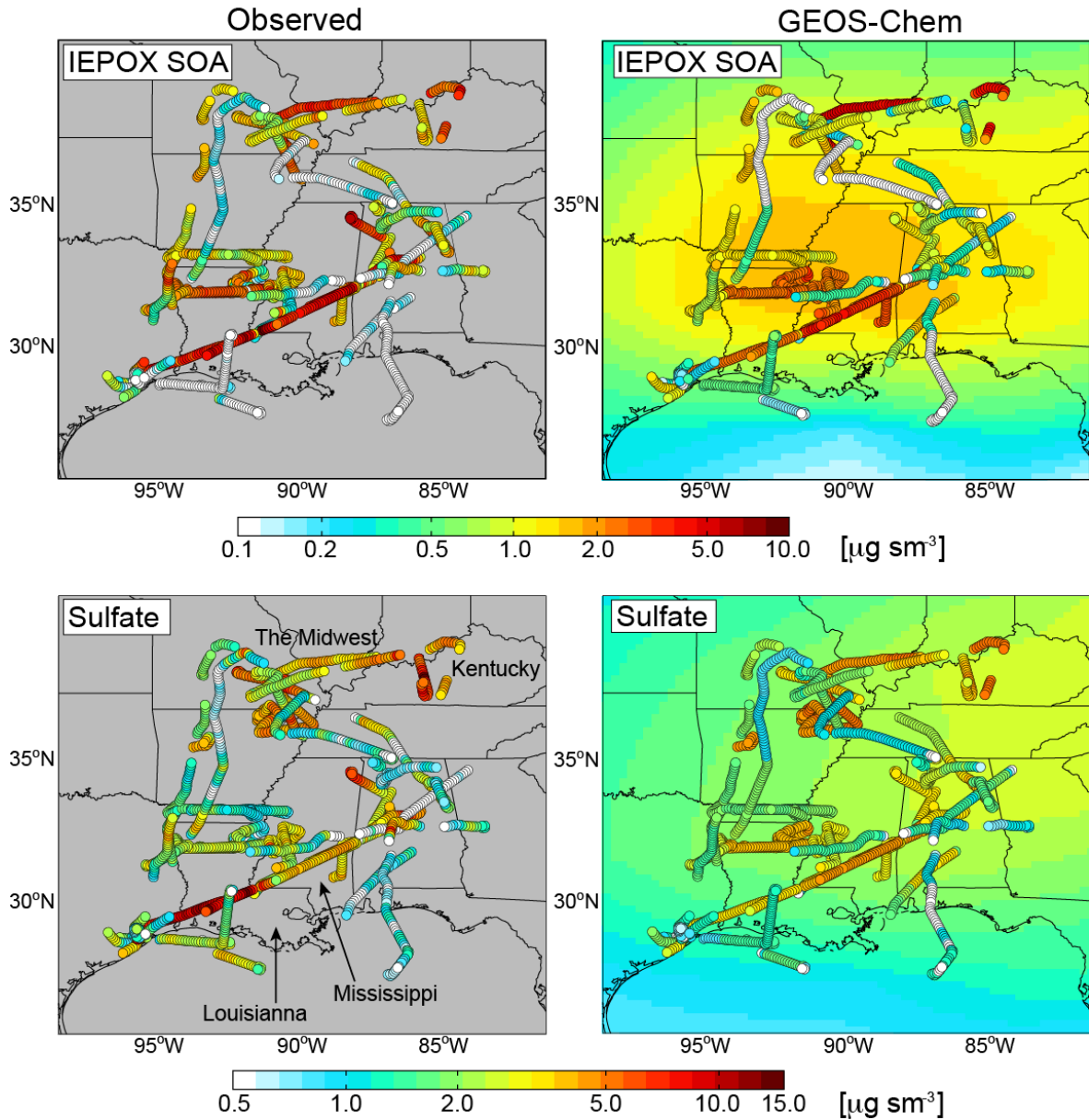
1037 **Figure 4.** Time series of the concentrations of isoprene SOA components at the SOAS site in
 1038 Centreville, Alabama (32.94°N; 87.18°W) in June-July 2013: measured (black) and modeled
 1039 (red) IEPOX SOA (top) and C₅-LVOC SOA (bottom) mass concentrations. Means and 1σ
 1040 standard deviations are given for the observations and the model.



1041

1042 **Figure 5.** Relationship of IEPOX SOA and sulfate concentrations over the Southeast US in
 1043 summer. Observed (black) and simulated (red) data are averages for each campaign day during
 1044 SOAS (left), and boundary layer averages (< 2 km) for $2^\circ \times 2.5^\circ$ GEOS-Chem grid squares on
 1045 individual flight days during SEAC⁴RS (right). RMA regression slopes and Pearson's correlation
 1046 coefficients are shown. 1σ standard deviations on the regression slopes are obtained with
 1047 jackknife resampling.

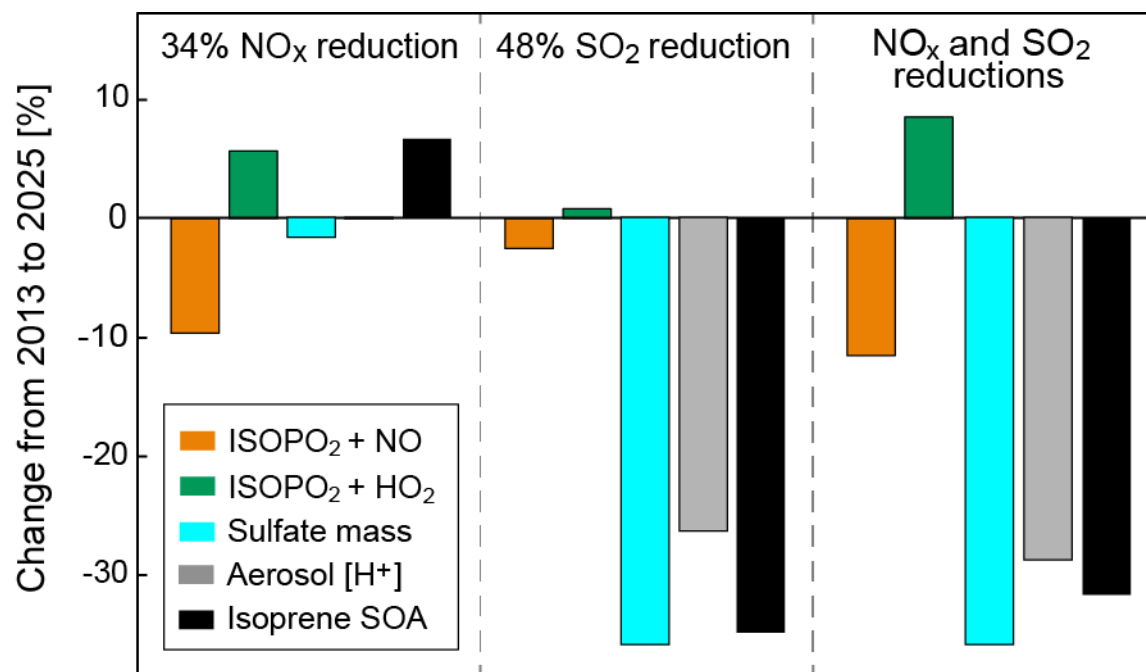
Boundary-layer IEPOX SOA and Sulfate Concentrations



1048

1049 **Figure 6.** Spatial distributions of IEPOX SOA and sulfate concentrations in the boundary layer
1050 (<2 km) over the Southeast US during SEAC⁴RS (August-September 2013). Aircraft AMS
1051 observations of IEPOX SOA (top left) and sulfate (bottom left) are compared to model values
1052 sampled at the time and location of the aircraft observations (individual points) and averaged
1053 during the SEAC⁴RS period (background contours). Data are on a logarithmic scale.

1054



1055

1056

1057 **Figure 7.** Effect of projected 2013-2025 reductions in US anthropogenic emissions on the
 1058 formation of isoprene secondary organic aerosol (SOA). Emissions of NO_x and SO₂ are projected
 1059 to decrease by 34% and 48%, respectively. Panels show the resulting percentage changes in the
 1060 branching of ISOPO₂ between the NO and HO₂ oxidation channels, sulfate mass concentration,
 1061 aerosol [H⁺] concentration, and isoprene SOA mass concentration. Values are summer means for
 1062 the Southeast US boundary layer.

1063